DLR-IB-FT-BS-2022-110

Extension of a helicopter aerodynamics model by unsteady stall effects

Interner Bericht Hochschulschrift

Autor: Shaik Asif

Deutsches Zentrum
DLR für Luft- und Raumfahrt

Institutsbericht
IB 111-2022-110

Extension of a helicopter aerodynamics model by unsteady stall effects

Shaik Asif

Institut für Flugsystemtechnik
Braunschweig

069	Seiten
015	Abbildungen
005	Tabellen
038	Referenzen

Deutsches Zentrum für Luft- und Raumfahrt e.V.
Institut für Flugsystemtechnik
Abteilung Hubschrauber

Stufe der Zugänglichkeit: I, Allgemein zugänglich: Der Interne Bericht wird elektronisch ohne Einschränkungen in ELIB abgelegt. Falls vorhanden, ist je ein gedrucktes Exemplar an die zuständige Standortbibliothek und an das zentrale Archiv abzugeben.

Braunschweig, den 12.09.2022

Unterschriften:

Institutsdirektor:	Prof. Dr.-Ing. S. Levedag	
Abteilungsleiter:	Dr.-Ing. Klausdieter Pahlke	
Betreuer:	M.Sc. Maximilian Mindt	
Verfasser:	Shaik Asif	

Extension of a helicopter aerodynamics model by unsteady stall effects

Studienarbeit

Deutsches Zentrum für Luft- und Raumfahrt (DLR)

Institut für Flugsystemtechnik

Name	: Shaik Asif
Course	: Computational Sciences in Engineering M.Sc.
Matriculation number	: 5026864
Date	: 23.05.2022

Professor	: Habl. Dr.-Ing. Stefan Langer
Betreuer	: M.Sc Maximilian Mindt

Registration of Specialisation Project (PRO)

Date of Registration:	08/11/2021.
Date of Submission:	07/05/2022

Student

ASIF, SHAIK

Last Name, First Name

Year of Enrollment: 2019   Matriculation #: 5026864

Examiner

_____

Last Name, First Name

_____

Institute

Title of Specialisation Project (German)

Title of Specialisation Project (English)

Extension of a helicopter aerodynamic model by unsteady stall effects

After submit their paper students have to hold their presentation (10% of the final grade).

Stefan 4

Date & Signature Examiner

08/11/2021,

Date & Signature Student

Submit this form and the task sheet to CSE via email (cse-office@tu-braunschweig.de) cc-ing your examiner.

2

Registration of Specialisation Project (PRO)

Specialisation project at a glance:
- Duration: maximum of 26 weeks
- Presentation (10% of final grade)
- Generally during 3rd semester

For more details, please refer to the module handbook.

Please be aware that you may not re-purpose any part of the specialisation project during your master thesis as is stated in the additional part of the examination regulations §6 sec. 3.

> "(3) The Master's thesis carries 30 credits and has to be completed within six months. In their Master's thesis, students shall treat a topic within their chosen specialism that is noticeably different from the subject of the specialisation project in terms of method and content."
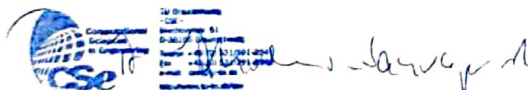
For any questions or queries, please reach out to the CSE office via:

Phone: +49-531-391-2241
Email: cse-office@tu-braunschweig.de

TU Braunschweig - CSE
Beethovenstr. 51
38106 Braunschweig

Kind Regards,

Anne Ahrens-Sauvagerd

FAQs

May I write my PRO at a company?
Yes, you may. However, a professor of the TU Braunschweig has to be your examiner and will also be responsible signing your registration form, task and grade sheet.

Do I have to submit the form "Registration of Specialization Project"?
Yes, you have to submit this form in order to start your PRO. The examination board has ruled that starting July 1, 2020 all CSE students have to submit the form plus the task sheet to the CSE office.

What do I need to submit to register my PRO with CSE?
You have to submit
1. Form "Registration of Student Project"
2. Task Sheet

Submit to CSE office via email cse-office@tu-braunschweig.de

Do I have to submit the original hard copy, or does a soft copy via email suffice?
A soft copy sent to CSE office cc-ing the examiner suffices.

Topic of an assignment for Shaik Asif

Title: Extension of a helicopter aerodynamics model by unsteady stall effects

Subject: The Institute of Flight Systems of DLR is modelling rotors of helicopters and wind turbines since many years and has gained unique knowledge in this field. The competence includes modelling of the rotor blade dynamics, the blade airfoil aerodynamics as well as the rotor downwash. Currently, a new comprehensive simulation program for the aeromechanics of helicopters named VAST – Versatile Aeromechanics Simulation Tool – is being developed. The activities involve the development and implementation of numerical methods for the simulation and analysis of dynamic systems, the graphical user interface, data visualization as well as modelling of physical effects in structural dynamics, flight mechanics and aerodynamics.

The aerodynamics of rotor blade airfoils can be calculated via a table look up method or the model proposed by Leiss with the adaptions published by Mindt [1] in VAST. In both variants, the model developed by Leishman and Beddoes [2] is used to calculate the effective angle of attack and the noncirculatory forces in unsteady conditions. What is missing for a usage of the Leishman-Beddoes model on its own is the inclusion of nonlinear and stall effects. The associated extension of the existing implementation shall be done in this assignment. Furthermore, the proper functioning of the complete model shall be proved.

Tasks:

- Literature research regarding indicial aerodynamics and the aerodynamic model by Leishman and Beddoes
- Familiarization with code development in VAST
- Inclusion of unsteady stall effects into the existing model parts in the simulation tool VAST
- Verification of the model and safeguarding the implementation via unit tests
- Investigation of differences to the existing formulations
- Documentation of results

Supervisor:

Maximilian Mindt
Institut für Flugsystemtechnik / Abteilung Hubschrauber
Deutsches Zentrum für Luft- und Raumfahrt e.V.
Lilienthalplatz 7
38108 Braunschweig
Mail: Maximilian.mindt@dlr.de
Tel: 0531 295 2698

[1] Mindt, M., "Merging an Analytical Aerodynamic Model for Helicopter Applications with a State-Space Formulation for Unsteady Airfoil Behavior," 67. Deutscher Luft- und Raumfahrtkongress, September 2018
[2] J. G. Leishman and G. L. Crouse Jr. "A State-Space Model of Unsteady Aerodynamics in a Compressible Flow for Flutter Analyses". In: 27th AIAA Aerospace Sciences Meeting. Reno, Nevada, 1989.

Acknowledgments

Declaration in lieu of oath

I declare that I have written the presented Studienarbeit/Student Thesis independently, without any unauthorized outside help or advice and only by using the scientific aids and literature specified.

Braunschweig, 23.05.2022   Shaik Asif

Abstract

Keywords: Nonlinear Effects, Dynamic Stall, Leishman-Beddoes, Leishman-Crouse, Indicial Method, TES, LES

Presently a comprehensive simulation program for the aeromechanics of helicopters named VAST – Versatile Aeromechanics Simulation Tool – is being developed by the Institute of Flight Systems of DLR. This work aims to include the indicial response model to compute the 2D airfoil lift, pitching moment, and chord force for rotor air loads prediction in VAST. Leishman and Crouse developed the state-space formulation for Leishman and Beddoe's indicial response method. The state-space formulation accounts for the attached and separated flow and respective circulatory and non-circulatory loading effects. Non-linear effects produced due to the Trailing Edge Separation (TES) are accounted by modifying the Kirchhoff flow. The onset of the Leading Edge Separation (LES) or Shock-induced separation was denoted by a generalized criterion. However, the VAST model uses two extra states. One to track the non-dimensional vortex travel time and another for the track direction of airfoil pitching. To get the progressive transition from the vortex lift strength accumulation and exponential decay. The results are validated with experimental data and the Leishman-Crouse model data for stall onset, moderate and deep dynamic stall conditions from Leishman-Crouse [LC89], and a reasonable to a good agreement was found.

Table of Contents

Designations

Symbol	Units	Description
a	m/s	Sonic velocity
A	m^2	Area of the airfoil
A	-	Internal connectivity of states matrix
A_n	-	Coefficients of indicial functions
a_{ij}	-	Elements of the system state matrix
B	-	States with external input effects matrix
b	m	Semi-chord length
b_n	-	Exponents of indicial functions
C	-	System output matrix
c_{ij}	-	Elements of the system output matrix
c	m	Airfoil chord
$C(k)$	-	Theodorsen function
C_C	-	Chord force coefficient
C_D	-	Pressure drag coefficient
C_{D0}	-	Zero Pressure drag coefficient
C_M	-	Pitching moment about the 1/4th chord
C_{M0}	-	Zero lift pitching moment coefficient
C_N	-	Normal force coefficient
$C_{N_{max}}$	-	Maximum normal force coefficient
C_{N_1}	-	Critical normal force coefficient
C_{N_α}	-	Normal force curve slope
C_p	-	Pressure coefficient
CP_v	-	Vortex lift center of pressure
f, f', f''	-	Separation point location
D	-	feed forward matrix
F	N	Resultant force
h	m	Plunging (heaving) displacement, positive downwards
k	-	Reduced frequency
K_0	-	Aerodynamic center offset
K_1	-	Constant for direct effect on COP
K_2	-	Coefficient for shape of the moment break

Designation

Symbol	Units	Description
K	-	noncirculatory force time constant
L	N	Section lift
M	-	Mach number
P	Pa	Pressure at a point
q	-	Nondimensional pitch rate $= \frac{\dot{\alpha}c}{V}$
R	m	Blade radius
S	-	Distance travelled in semi-chords $= \frac{2Vt}{c}$
S_n	-	Stall characteristics
t	s	Time
t	m	Maximum airfoil thickness
T_I	-	Noncirculatory time constant $= \frac{c}{a}$
T	-	Time constant
U	m/s	Resultant velocity at blade
U_∞	m/s	Free-stream velocity
u	-	System inputs
V	m/s	Local velocity
V_n	m/s	Normal velocity of vortex
w_0	-	Gust load
x_i	-	Vector of State variables
y	-	Vector of output
X_n, Y_n	-	recurrence functions

Designation

Greek Symbol	Units	Description
α	rad	Angle of attack (AoA)
$\alpha_{L=0}$	rad	AoA for zero lift for cambered airfoil
α_E	rad	Effective angle of attack
α_1	rad	Break point for f=0.7
$\dot{\alpha}$	rad/sec	pitch rate
$\ddot{\alpha}$	rad/sec^2	angular acceleration
β	-	Compressibility factor $= \sqrt{1 - M^2}$
γ	-	Circulation
$\delta(t)$	-	Dirac delta function
η	-	Efficiency factor
μ	kg/ms	Dynamic viscosity
ρ	kg/m^3	Density of air
τ	-	Time constant
ϕ	-	Indicial response function
Φ	-	Potential function
$\phi(s)$	-	Wagner function
Ψ	-	Stream function
$\Psi(s)$	-	Küssner function

Subscripts	-	Description
$(.)_{1/4}$	-	Quarter chord
$(.)_{3/4}$	-	Three-quarter chord
$(.)_M$	-	Refers to pitching moment about quarter chord
$(.)_q$	-	Refers to pitch rate
$(.)_\alpha$	-	Refers to angle of attack

Superscripts	-	Description
$(.)^C$	-	Refers to circulatory loading
$(.)^I$	-	Refers to non-circulatory (impulsive) loading
$(.)^P$	-	Refers to potential (attached flow) loading
$(.)^f$	-	Refers to loads with trailing edge separation
$(.)^v$	-	Refers to vortex loading

Abbreviation	Description
AIAA	American Institute of Aerospace and Aeronautics
AoA	Angle of Attack
BC	Boundary Condition
CFD	Computational Fluid Dynamics
COP	Center of Pressure
DLR	Deutsches Zentrum für Luft- und Raumfahrt
FP	Flate Plate
LE	Leading Edge
LES	Leading Edge Separation
LEV	Leading Edge Vortex
NACA	National Advisory Committee for Aeronautics (now NASA)
NC	Non-circulatory component
ODE	Ordinary Differential Equation
TE	Trailing Edge
TES	Trailing Edge Separation
VAST	Versatile Aeromechanics Simulation Tool

List of Figures

List of Tables

1 Introduction

As stated by *Igor Ivanovitch Sikorsky*, "The idea of a vehicle that could lift itself vertically from the ground and hover motionless in the air was probably born at the same time that man first dreamed of flying". We have come a long way in the development of rotary-wing aircraft. The science of aerodynamics played a major role during the timeline of the development of rotary-wing aircraft. This Studienarbeit work is related to implementing and validating the Leishman-Beddoes dynamic stall model in the Versatile Aeromechanics Simulation Tool (VAST) developed by Institut für Flugsystemtechnik, DLR.

1.1 Motivation

The helicopter's main rotor understanding is essential as it is a crucial component and responsible for the vertical lift and horizontal propulsive force in forward flight and controls the attitude and positions of the helicopter. Hence it is necessary to study the rotor aerodynamic performance. Dynamic stall is an essential driver in predicting the rotor air loads performance. An accurate prediction of rotor airfoil behavior will help in better rotor design and optimizing flight operation. Helicopter performance is mainly restricted due to the excessive blade stresses and control loads arising from airfoil stall flutter on the retreating blade. This phenomenon occurs due to the interaction of the transient pitching moment deviations due to the separated flow effects of the dynamic stall and the blade torsional degree of freedom. It is necessary to consider the dynamic effects on the stall, because generally their magnitude influence the choice of both airfoil and their placement and the dynamic structural characteristics of the rotor blade.

Predicting the airfoil performance under the dynamic stall requires low fidelity advanced engineering empirical and semi-empirical models or high fidelity sophisticated computational fluid dynamics models (CFD). High-fidelity CFD methods being more accurate than empirical models have the downside of being computationally expensive; therefore, they are not the first preference of rotor design analysts. The semi-empirical models are a computationally efficient alternative to CFD codes; however, they need extensive validation with test results and experimental test data for static airfoil behavior for different airfoils for a range of Mach numbers. Aerodynamic researchers have developed fairly sophisticated semi-empirically based models (e.g. Ref. [Bed76], [TP80], [Gan83], and [LB86]). These semi-empirical models perform well for unsteady effects under attached flow conditions. However,

for the dynamic stall, they heavily rely on the synthesization of wind tunnel data from unsteady airfoil tests.

1.2   Aims and Objectives

In VAST, the aerodynamics of rotor blade airfoils can be calculated via a table look-up method or the model proposed by Leiss with the adaptions published by Mindt ([Min18]). In both variants, the model developed by Leishman and Beddoes [LB86] is used to calculate the effective angle of attack and the non-circulatory forces in unsteady conditions. What is missing for the usage of the Leishman-Beddoes model on its own is the inclusion of nonlinear and stall effects. The associated extension of the existing implementation shall be done in this assignment. Furthermore, the proper functioning of the complete model shall be proved.

1.3   Methodology

The focus of this work was to implement a Leishman-Beddoes model in VAST to predict the aerodynamic performance under the dynamic stall condition. Before running the dynamic stall model, the airfoil dependent model parameters selected from the literature were used.

The first phase of the work was to carry out literature research regarding indicial aerodynamics and the aerodynamic model by Leishman and Beddoes. The second phase of the work started with familiarization with code development in VAST and understanding the already existing aerodynamic models. In the third phase of the work, the inclusion of unsteady stall effects into the existing model in the simulation tool VAST is performed. In the fourth phase of the work, verification of the model is completed. Finally, documenting the results.

1.4   Outline

The report starts with a brief introduction of the theoretical background of the studienarbeit and then discusses the work done in the literature in Chapter 2. Chapter 3 discusses the general indicial response and Leishman-Beddoes state-space model formulation for attached flow and dynamic stall conditions for unsteady compressible flow. Chapter 4 deals with validating the implemented model with standard test cases. Finally, chapter 5 provides conclusion and outlook of the work.

2 State of the Art

As stated by I. E. Garrick, "The addition of the dimension 'time' to steady aerodynamic has far-reaching effects, both practical and theoretical. There is the practical necessity of coping with many important problems involving non-steady phenomena such as flutter, buffeting, transient flows, gust, dynamic response in flight, maneuvers, and stability. Apart from the many applications, theoretical non-steady aerodynamics embraces and sheds light on the realm of steady aerodynamics and introduces new methods."

This chapter provides an overview of the theoretical framework and research that has been done in the unsteady aerodynamics field. It starts with a brief overview of the unsteady aerodynamics of the helicopter rotor. Followed by introducing the most common models that deal with unsteady effects. Finally, an overview of the state-space model and VAST tool is given.

2.1 Unsteady Aerodynamics of the Helicopter Rotor

As stated by J.G. Leishman, the unsteady aerodynamics can be defined as, "If the motion, or the flow around; of an airfoil or a wing in a free stream, changes by time, so do the acting aerodynamic loads. When the changes in the motion or flow-field structure are fast enough, the unsteady aerodynamic effects can not be neglected".

Rotating blades are always a challenge for aerodynamicists because of the flow field's highly unsteady and three-dimensional nature. Rotating blades encounters complex flowfield structure like inflow, sweep, wake distortion, and other disturbance, as shown in figure 2.1. the airfoil can experience unsteady effects both in the case of attached flow and separated flow. The *degree of unsteadiness* of an airfoil can be represented with the parameter *reduced frequency (k)*. It is obtained through dimensional analysis of resultant force (F) on an airfoil of chord (c), oscillating at an angular frequency (ω) of velocity (V), the unsteadiness can be classified using k as shown in Table 2.1.

$$\frac{F}{\rho V^2 c^2} = f\left(\frac{\rho V c}{\mu}, \frac{V}{a}, \frac{\omega c}{2V}\right) = f(R_e, M, k) \qquad (2.1)$$

The *Reduced frequency* parameter k can be represented interms of semichord as shown in equation 2.2.

$$k = \frac{\omega c}{2V} \tag{2.2}$$

nature of flow	unsteady parameter (k)
Steady	0
Quasi-steady	$0 \leq k \leq 0.05$
Unsteady	$0.05 \leq k \leq 0.2$
Highly unsteady	$k \geq 0.2$

Table 2.1: Types of flow based on unsteadiness parameter k
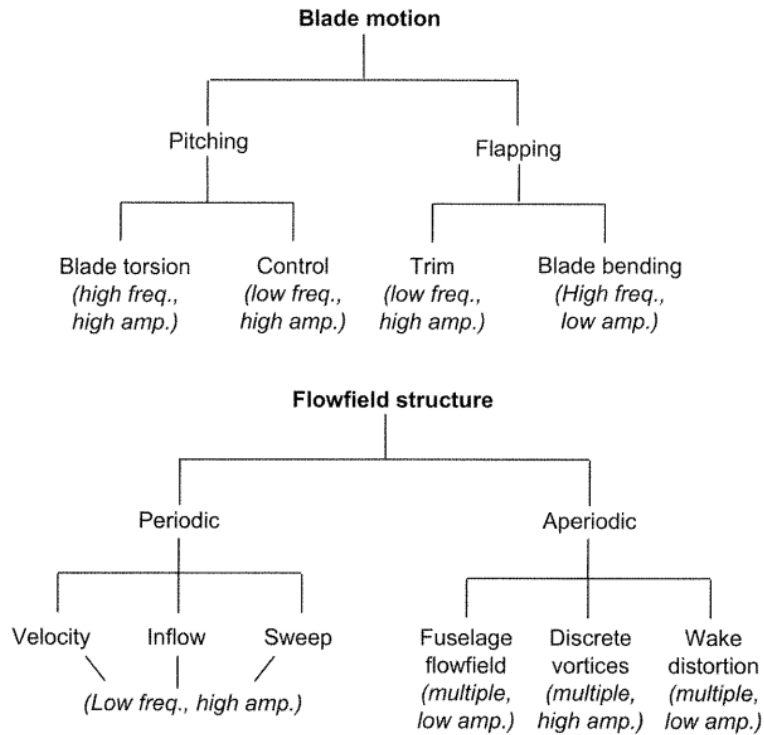
Figure 2.1: Possible sources of unsteady aerodynamic loading on a helicopter rotor (Ref. [Bed80]).

The lifting capability of any part of the blade depends on local angle of attack (AoA). When the AoA exceeds the stall boundary, the flow separation occurs on the airfoil's upper surface, which abruptly changes the aerodynamic response. The main rotor is divided into two sides during the helicopter's

forward flight. Namely, the advancing side (0° to 180° where the local velocity of the blade is added up with the incoming flow velocity) and then followed by the retreating side (180° to 360° where the local flow velocity is subtracted from incoming flow velocity) as shown in figure 2.2 ([Lei00]). The lift produced on the advancing side of the disk must be balanced by the lift generated on the retreating side. But due to lower velocity at the retreating side, the blade must operate at a higher angle of attack (AoA). When this AoA required for trim does not exceed the stall angle and the follow is attached, the blade performance is described by steady aerodynamics; otherwise, it will cause a stall of an airfoil. In the case of a helicopter rotor, blades experience unsteady forces from different sources, as shown in figure 2.1 and this causes the flow separation, which leads to the dynamic stall of the blade.
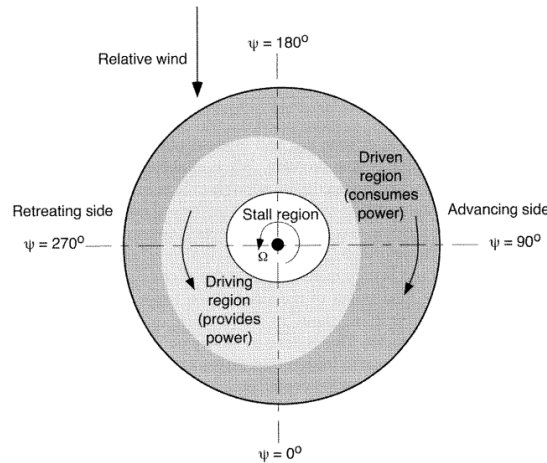
Figure 2.2: Forward flight (Ref. [Lei00])

A prerequisite in any unsteady aerodynamic theory is the ability to model the unsteady air loads accurately at the blade element under attached flow conditions ([Lei00]). The most fundamental approach to modeling the unsteady aerodynamic effects is the extension of the steady, 2D thin airfoil theory. Thin-Airfoil theory is a base for all the classical unsteady flow theories such as Wagner([Wag24]), Theodorsen([The49]), Küssner([Küs36]), and von Karman and Sears ([KS38]). The model must satisfy the following two conditions to apply the thin airfoil theory, which ensures the incompressibility of the flow. First, the product of $Mk << 1$ ensures the low local velocity and low amplitudes of unsteadiness. Second, any model must be written in mathematical form for easy coupling with other models.

2.1.1 Dynamic Stall

The dynamic stall phenomenon has long been known to be a factor that limits helicopter performance. At the same time, in a single revolution of the rotor, the rotor blades experience different AoA on the advancing side and retreating side. Stall occurs on a rotor blade element in a dynamic and time-dependent manner when AoA results from cyclic pitch input, blade flapping, wake inflow, and separation changes continuously in the time domain and is referred to as dynamic stall.

The general dynamic stall definition by McCroskey [MCM76] is, "Dynamic stall will occur on any airfoil or other lifting surface when it is subjected to time dependent pitching, plunging or vertical translation, or the type of non steady motion, that takes the AoA above its normal static stall angle. Under this circumstances, the physics of flow separation and the development of stall have shown to be fundamentally different from the stall mechanism exhibited by the same airfoil under static condition (k=0)."

Leishman [Lei00] noted the characteristics of dynamic stall as follow (1) Dynamic stall is, in part, distinguished by a delay in the onset of flow separation to a higher AoA that would occur statically. (2) The initial delay in stall onset is advantageous as far as the performance and operational envelope is concerned. (3) It is characterized by the shedding of concentrated vortical disturbances from the leading edge airfoil region. (4) As long as these vortex disturbances remain on the upper surface, it acts to *enhance the lift* being produced. (5) The vortex flow pattern is not stable, and the vortex is quickly swept over the blade's chord by the oncoming flow. Vortex convection produces a rapid aft movement of pressure, which results in large nose-down pitching moments on the blade section and an increase in torsional loads on the blade.

Helicopter rotor blades experience significant fluctuations in AoA due to variations in inflow velocity. These large fluctuations in AoA near static stall result in delaying the onset of a stall to a much higher AoA than a static stall ([McC81]). Dynamic stall delays the onset of the stall and delays the reattachment of the flow after stall.

Leishman ([Lei00]) presented 5 sequential stages of the dynamic stall process as shown in figure 2.3. During the first stage, (5 to 1) AoA increases from the minimum value to the relative static stall value; the lift coefficient also increases following the static trend, and flow remains attached. During the second stage (1 to 2), the formation of re-circulations starts in the boundary layer near the trailing edge. Lift continues to increase, and LEV also develops

further. In stage three (2 to 3), the leading edge vortex starts to convect over the airfoil chord; the center of pressure also moves downstream till it reaches the trailing edge. This results in a large nose-down pitching moment called *moment break or moment stall*. During this stage, lift increases further and reaches the maximum value when the vortex reaches the airfoil's trailing edge. At stage four (3 to 4), the complete flow separation takes place, resulting in an abrupt decrease in lift and a decrease in AoA. Finally, in stage five (4 to 5), a delayed flow reattachment occurs.
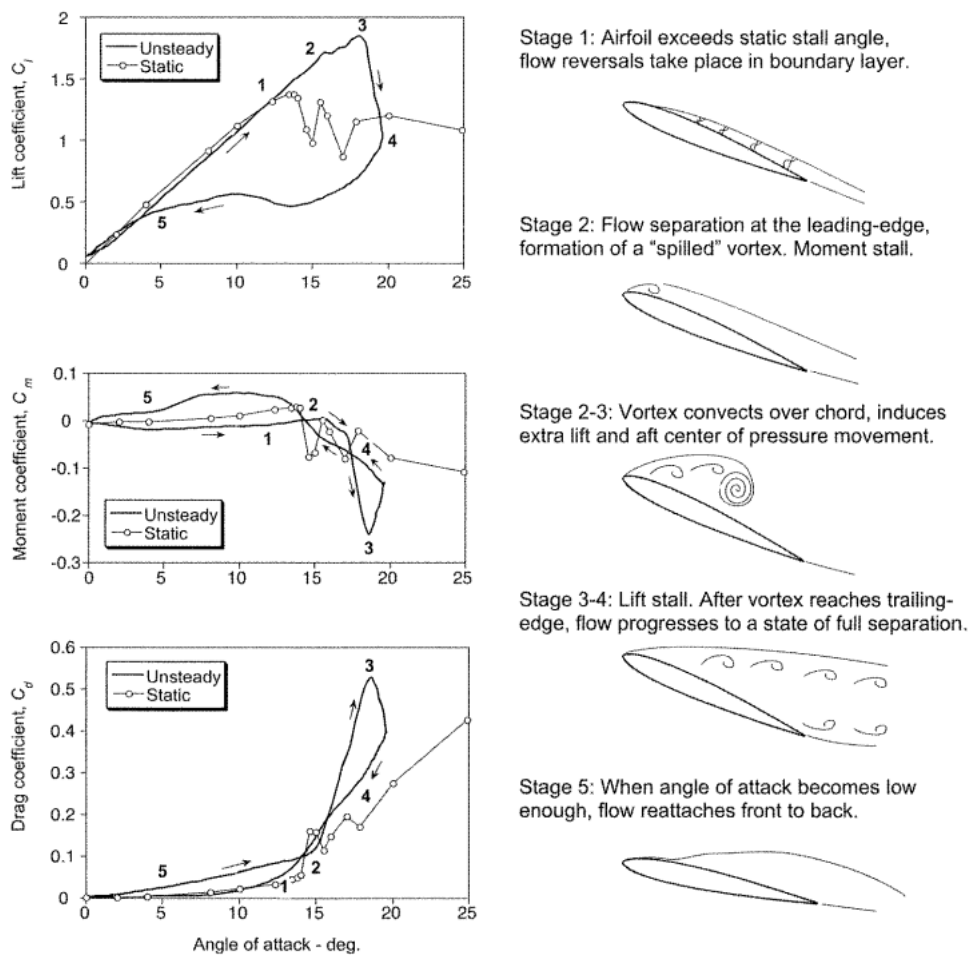
Figure 2.3: Schematic showing the essential flow morphology and the unsteady airloads during the dynamic stall of an oscillating 2-D airfoil. (Ref. [Lei00])

Mulleners and Raffel ([MR12]) presented that LEV generates small counter-rotating vortices at the trailing edge; when this vortices move towards the

leading edge cause the detachment of LEV from the airfoil surface, which is known as vortex-induced separation. McCroskey ([McC81]) classified the dynamic stall into two categories based on the extension of separation. First a light stall, and second a deep stall. Figure 2.4 shows the physical representation for light stall and deep stall.

(a) light stall   (b) deep stall
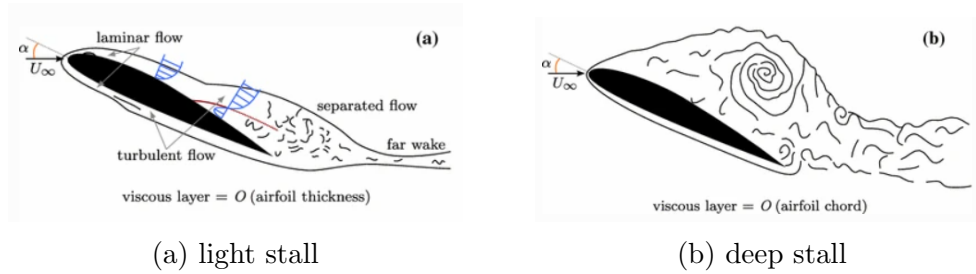
Figure 2.4: Topology of (a) light and (b) deep stall configuration. (Ref. [MP82])

2.2 High Fidelity Aerodynamic Models

The most traditional and well-known approach to finding the aerodynamics parameters is computational fluid dynamics models (CFD). CFD methods are based on classical *Navier-Stokes* equations and are based on conservation laws such as mass, momentum, and energy conservation. There are different types of CFD models available based on the problem one is solving.

Many turbulence models are available to obtain closure of numerical solutions; the RANS method is most commonly used in CFD to solve flow-field variables. A more superior and computationally expensive method is Large Eddy Simulation (LES). LES uses spatial averaging over temporal to resolve large coherent structures in the flow field while small, turbulent structures are modeled. The most accurate and computationally expensive method in CFD is Direct Numerical Simulation (DNS). DNS resolves turbulence on all scales. Large-scale turbulence is used for accounting for the forcing scales and the Kolmogorov scale to account for turbulent energy dissipation into heat. Figure 2.5 shows the comparison of RANS, LES, and DNS.

2.3 Low Fidelity Aerodynamics Models

2.3.1 Thin Airfoil Theory

Mirnal Kaushik [Mir19] states that, "Thin airfoil theory is a straightforward hypothesis of airfoils that relates angle of attack to lift for an incompressible
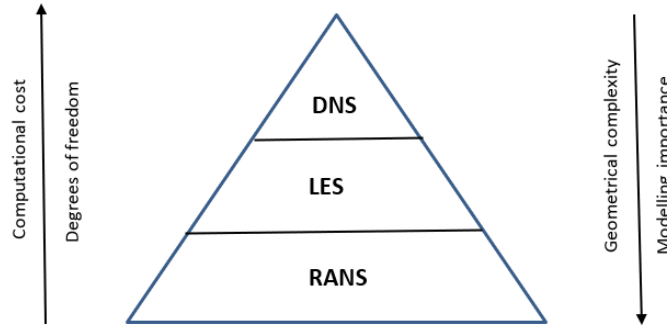
Figure 2.5: Turbulence models in CFD

and inviscid flow past an airfoil. This theory idealizes the flow past an airfoil as two-dimensional stream around a thin airfoil which can be envisioned as tending to an airfoil of zero thickness and infinite wingspan." Governing equations and boundary conditions *(No penetration BC)* for thin airfoil theory are as follows:

$$\nabla^2 \Phi = 0 \tag{2.3}$$

$$\nabla^2 \Psi = 0 \tag{2.4}$$

$$\nabla^2 (\Phi + i\Psi) = 0 \tag{2.5}$$

$$V_n = 0, \quad W(x, 0) = 0$$

Where (2.3) is the condition for potential function, (2.4) is the condition for streamline function and (2.5) is the condition for potential flows. $V_n = 0$ is the condition for velocity component and $W(x, 0) = 0$ shows the circulation at different location along the chord.

The integral form of the vortex strength in thin airfoil theory is as shown in the equation 2.6, and the solution for the strength of the vorticities from the integral equation obtain by Fourier analysis is as shown in the equation 2.7. One can find the coefficient of lift and moment using the equations 2.8 and 2.9 respectively.

$$\frac{1}{2\pi} \int_0^\pi \frac{\gamma(x\prime) dx\prime}{(x - x\prime)} = U_\infty sin\left(\alpha - \frac{dz_c}{dx}\right) \tag{2.6}$$

$$\gamma(\phi) = 2U_\infty \left(A_0 \frac{1 + cos(\phi)}{sin(\phi)} + \sum_{n=1}^{\infty} A_n sin(n\phi) \right) \qquad (2.7)$$

$$Where \quad A_0 = \alpha - \frac{1}{\pi} \int_0^\pi \frac{dz}{dx} d\phi_0 \quad A_n = \frac{2}{\pi} \int_0^\pi \frac{dz}{dx} cos(n\phi_0) d\phi_0$$

$$C_l = \frac{2 \int_0^c \gamma(x) dx}{U_\infty c} = 2\pi \left(A_0 + \frac{A_1}{2} \right) = 2\pi(\alpha - \alpha_{L=0}) \qquad (2.8)$$

$$C_{m_{c/4}} = C_{m_{ac}} = \frac{\pi}{4}(A_2 + A_1) \qquad (2.9)$$

$$Where \quad \alpha_{L=0} = \alpha - A_0 - \frac{1}{2}A_1$$
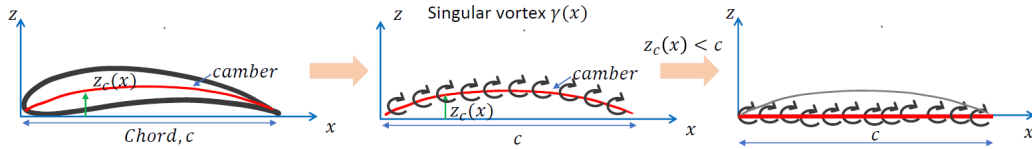
Figure 2.6: Thin airfoil theory

2.3.2 Indicial Response: Wagner Model

Unsteady aerodynamics extends the thin airfoil theory to include the wake from the sudden impulsive start of the airfoil. *Wagner* first studied the starting wake effect and obtained the solution to the impulsively started flat plate problem ([Wag24]). He showed that delay in circulation growth for an accelerating wing at angle of attack below steady-state stall and wing's starting vortex induces a downwash on the wing, which reduces the local angle of attack. This effect diminishes as the starting vortex moves away from the wing and leads to an asymptotic rise in wing lift with time.

Wagner considered a horizontal line of a continuous distribution of vorticity points shed from the trailing edge, ending with the starting vortex, and the flat plate is also horizontal, as shown in Fig. 2.7. At the same time, the free stream is inclined by a small angle α. The vortices are ejected at the ith time instance and then travel at the free stream airspeed, such that $\Delta x = U\Delta t$. Their strength *does not change* as they travel downstream. Finally, The vorticity distribution becomes continuous as $\Delta x \longrightarrow 0$.

Wagner's mathematical model expression for a lift on a thin airfoil undergoing a sudden change in AoA is as shown in equation 2.10. The first term is an apparent mass term, and the second term is the steady-state lift coefficient, with Wagner's function representing the effect of the wake. Unfortunately, the lack of a convenient and readily-usable expression for the Wagner function has resulted in the formulation of a variety of simplifying approximations that can be used in place of the exact form, such as R. T. Jones ([Jon40]) approximation.

Plot of Wagner's function *vs* semi-chord distance travelled is as shown in figure 2.8. The lift jumps to half the steady-state value in the first instance, increasing asymptotically towards the steady-state value.

$$C_l = \underbrace{\frac{\pi c}{2u}\delta(t)}_{\text{infinte pulse due to added mass ignored}} + \underbrace{2\pi\alpha\Phi(s)}_{\text{steady state lift with wagner's function}} \tag{2.10}$$

$$\Phi(s) = 1.0 - 0.165e^{-0.0455s} - 0.335e^{-0.3s}$$
$$s = \frac{Vc}{2t} \tag{2.11}$$
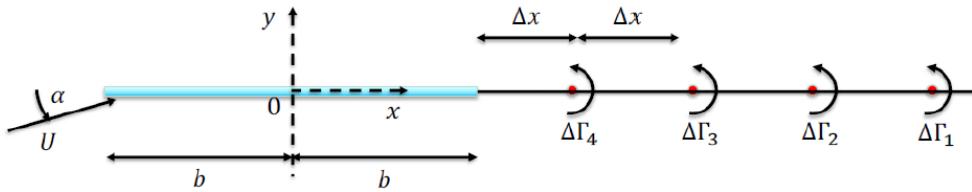
Figure 2.7: Wagner extension of thin airfoil model with wake

2.3.3 Duhamel Superposition

Mazelski Ref. [Maz51] and [MD52] appear to have been one of the first researchers to use exponential approximation to the indicial response for compressible flow. A similar approach has been adopted by Dowell Ref. [Dow80] to obtain the approximation for the indicial response for incompressible flow
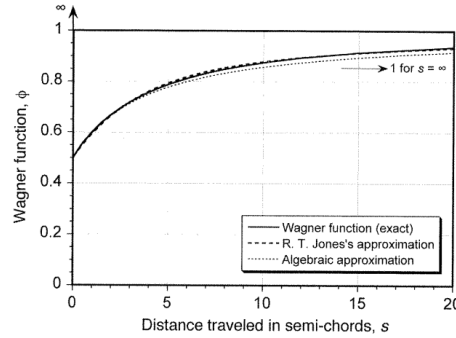
Figure 2.8: Wagner function for a step change in angle of attack (ref. [Lei00])

using Theodorsen's Ref. [The49] result and for compressible flow by using the Wagner's Ref. [Wag24] result with frequency response data from Williams Ref. [Wil80].

As shown by Jones Ref. [Jon40], the approximate aerodynamic transfer function equation 2.11 for the Wagner function contains two poles. Therefore, by increasing the number of poles, a more approximate indicial response function can be obtained, as shown by Venkatesan ([VF86]). However, more poles require more states and are computationally costly.

A general form of the aerodynamic indicial response function is as follows:

$$\phi(S) = 1.0 - A_1 \exp\left(-b_1 S\right) - A_2 \exp\left(-b_2 S\right) \tag{2.12}$$

Where time is generalized as $S = 2Vt/c$, which corresponds to the relative distance traveled in terms of semi-chord.

C_f is the unsteady force coefficient acting on the airfoil and it is smooth, nonlinear function of AoA. The main underlying principle in the indicial response function is that flow can be linearized concerning the forcing function. If $\partial C_f / \partial \alpha$ is the linear time-invariant response, it does not depend on α and depends on the time after the step input is applied. Then for any arbitrary inputs in α, the value of C_f can then be expressed in terms of the Duhamel superposition integral as shown in equation 2.13.

$$C_f(t) = \underbrace{\frac{dC_f}{d\alpha}\alpha(0)\Phi_f(t)}_{\text{short time transient}} + \frac{dC_f}{d\alpha}\underbrace{\int_0^t \frac{d\alpha}{dt}(\sigma)\phi_f(t-\sigma)d\sigma}_{\text{Duhamel integral}} \tag{2.13}$$

Duhamel integral produces an aerodynamic quantity that contains all of the prior time-history information of what has happened to the aerodynamic response since the initial time. C_f value for the steady flow is as shown in equation 2.14 and for the time-varying value of the lift coefficient, $C_l(t)$ can be expressed as a function of angle of attack, $\alpha(t)$, in terms of Duhamel integral as

$$C_l(t) = C_{l\alpha} \left[\alpha(t_0)\phi(S) + \int_{s_0}^{s} \frac{d\alpha}{dt}(\sigma)\phi(S-\sigma)d\sigma \right] = C_{l\alpha}\alpha_e(t) \qquad (2.14)$$

$$Where \quad \alpha_e(S) = \alpha(S_0)\phi(S) + \sum_{i=1}^{\infty} \frac{d\alpha}{ds}(\sigma_i)\phi(S-\sigma_i)\Delta\sigma_i$$

Solving equation 2.14 is not affordable in rotor calculation but there are options available to solve it efficiently. Duhamel integral in equation 2.14 can be written numerically as shown in equation 2.16.

$$\alpha_e(S) = \alpha(S) - X(S) - Y(S). \qquad (2.15)$$

$$Where \quad X(S) = A_1 \int_{S0}^{S} \frac{d\alpha}{dS}(\sigma)e^{-b_1(S-\sigma)}d\sigma$$

$$Y(S) = A_2 \int_{S0}^{S} \frac{d\alpha}{dS}(\sigma)e^{-b_2(S-\sigma)}d\sigma$$

Integral in $X(S)$ and $Y(S)$ terms for time $S+\Delta S$ can be solved by considering different numerical algorithms. Figure 2.9 shows the relative computational cost for different numerical schemes with their order of error. Equation 2.16 shows $X(S)$ and $Y(S)$ are written interms of one-step recursive formulas that will be denoted by Algorithm D-1:

$$X(S) = X(S-\Delta S)e^{-b_1\Delta S} + A_1\Delta\alpha_S$$
$$Y(S) = Y(S-\Delta S)e^{-b_2\Delta S} + A_2\Delta\alpha_S \qquad (2.16)$$

$$\frac{1-e^{-b_1\Delta S}}{b_1} \approx \Delta S \qquad (2.17)$$

The error in this alogrithm arises from approximation as shown in equation 2.17 and this results in relative error in integral equation which is as follow:
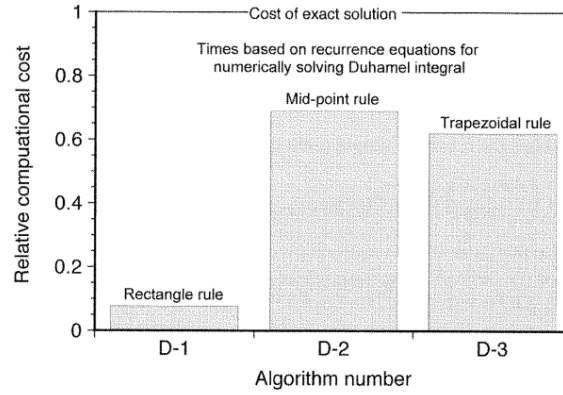
Figure 2.9: Relative computational cost of the numerical solution of Duhamel integral using different numerical methods. Cost is evaluated relative to exact solutions. (Ref. [Lei00])

$$\epsilon = 2 - \frac{b_1 \Delta S}{1 - e^{-b_1 \Delta S} - \frac{b_2 \Delta S}{1 - e^{-b_2 \Delta S}}} \tag{2.18}$$

2.3.4 Theodorsen Model

In 1949 Theodorsen ([The49]) came up with a more generalized harmonic unsteady flow around a flat plate by combining *translation, plunging (heaving) and pitching* motion. He divided the output lift into *non-circulatory lift* (due to translation, pitching, and plunging motion or added mass) and *circulatory lift* (due to circulation), as shown in block diagram in Fig. 2.10
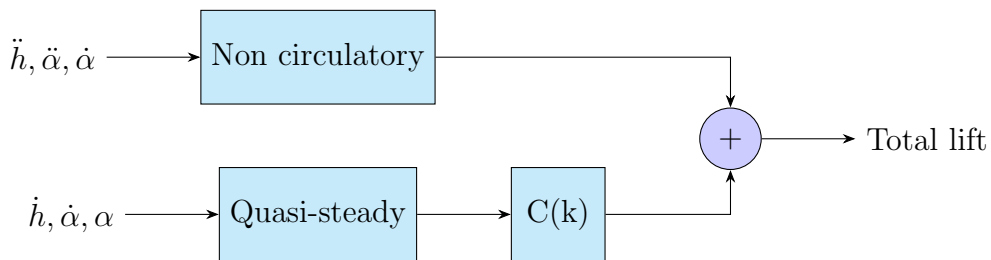
Figure 2.10: Theodorsen model

To obtain the lift's non-circulatory part, Theodorsen consider a streamline cylinder surface transformed it to a flat plat through conformal mapping as shown in figure 2.12 and he considered source singularities on the upper surface and sink singularities on the lower surface as shown in figure

2.11. However, the non-circulatory solution does not satisfy the *Kutta condition*. Theodorsen accomplished this by using the bound vortices inside the cylinder and the wake of counter-rotating vortices continually moving away, as shown in figure 2.12. Theodorsen's total lift is sum of circulatory lift and non-circulatory lift as shown in equation 2.20. Figure 2.13a and 2.13b shows change in theodorsen's function with respect to the reduced frequency (k).
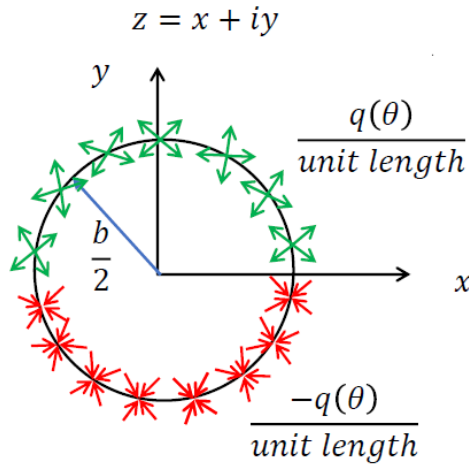
Figure 2.11: Sink and Source distribution on cylinder surface
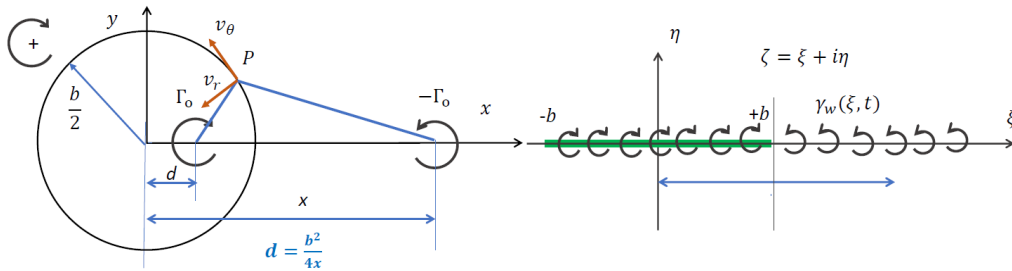
Figure 2.12: Bound vortex and wake effects (Ref. [The49])

$$L' = L'_{NC} + L'_C \tag{2.19}$$

$$L' = \underbrace{\pi\rho b^2(U_\infty\dot{\alpha} + \ddot{h} - \ddot{\alpha}ab)}_{\text{non-circulatory}} +$$

$$\underbrace{\rho U 2\pi b \left[\dot{h} + U\alpha + b\left(\frac{1}{2} - a\right)\dot{\alpha}\right] C(k)}_{\text{circulatory}} \tag{2.20}$$

$$M'_{c/2} = \underbrace{\pi\rho b^2\left[ba\ddot{h} + Ub\left(\frac{1}{1} - a\right)\dot{\alpha} - b^2\left(\frac{1}{8} + a^2\right)\ddot{\alpha}\right]}_{\text{non-circulatory}} +$$

$$\underbrace{2\pi\rho U b^2\left(a + \frac{1}{2}\right)\left[\dot{h} + U\alpha + b\left(\frac{1}{2} - a\right)\dot{\alpha}\right] C(k)}_{\text{circulatory}} \tag{2.21}$$

$$where \quad C(k) = \frac{\int_1^\infty \frac{\xi^*}{\sqrt{\xi^{*2}-1}} e^{-ik\xi^*} d\xi^*}{\int_1^\infty \sqrt{\frac{\xi^*+1}{\xi^*-1}} e^{-ik\xi^*} d\xi^*}$$

Where L' is total lift, $M'_{c/2}$ is total moment, h is plunging (heaving) displacement, positive downwards, α is AoA, a is the ratio of hinge distace w.r.t mid chord, b semi-chord, $\dot{\alpha}$ is pitch rate around the hinge, $\dot{h}$ is plunging velocity and U_∞ is free-stream velocity.

2.3.5 Küssner Model

The rotor wake produces a highly nonuniform induced velocity field across the plane of the rotor disk. The blade element encounters this nonuniform vertical upwash/downwash as it rotates in this field. Hence it is crucial to distinguish appropriately the effects on the airloads arising from AoA changes from blade motion. Küssner ([Küs36]) studied the lift response on a thin airfoil entering a sharp-edged vertical gust and correctly solved by Von Karman and Sears ([KS38]). As shown in figure 2.14 (a) quasi-steady AoA changes progressively as the airfoil penetrates the gust front. The resulting variation in lift coefficient can be written as in equation 2.22. Küsnner function is as shown in equation 2.23 with real and imaginary parts. The approximate form of the küssner function was given by exponential approximation by Sears and Sparks ([Sea41]) as shown in equation 2.24 and algebraic approximations by Bislinghoff ([BAH13]) as shown in equation 2.25.
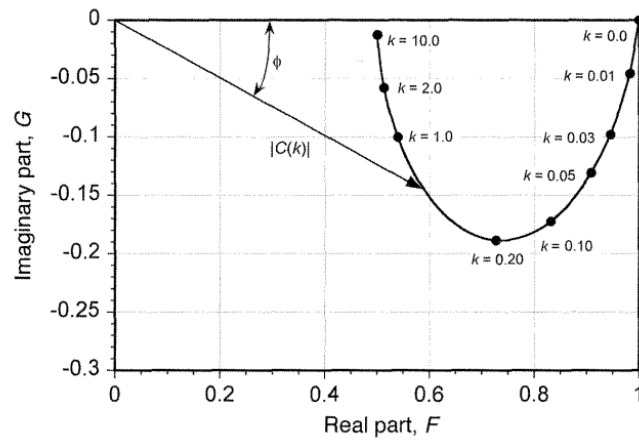
(a) Real and imaginary parts

Theodorsen's Function
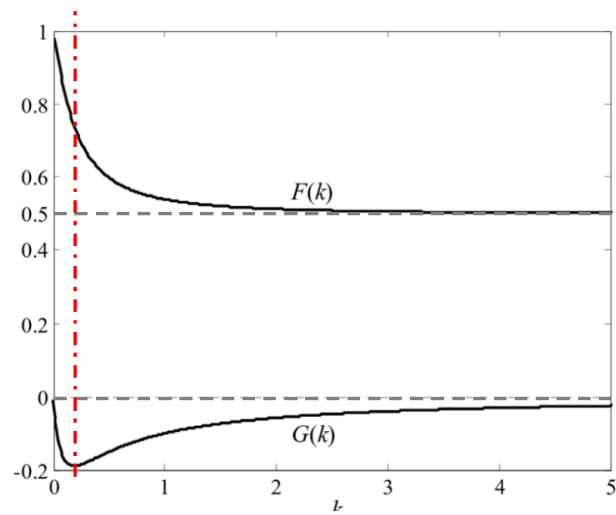
(b) Real and imaginary parts change with k

Figure 2.13: Theodorsen's function (Ref. [The49])

$$C_l(t) = 2\pi \left(\frac{w_0}{Y}\right) \Psi(s) \tag{2.22}$$

$$\Psi(s) = \frac{2}{\pi} \int_0^\infty \frac{[F_g(k) - G_g(k)] \, sin(ks)sin(k)dk}{k} \tag{2.23}$$
$$s > 0$$

$$\Psi(s) \cong 1 - 0.5e^{-0.13s} - 0.5e^{-s} \tag{2.24}$$

$$\Psi(s) \cong \frac{s^2 + s}{s^2 + 2.82s + 0.8} \tag{2.25}$$
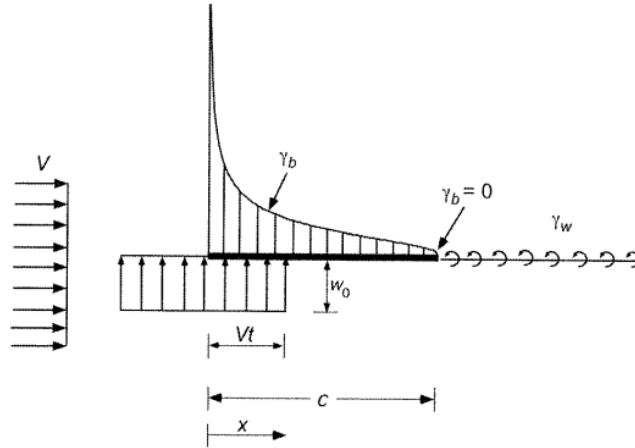
(a) Boundary conditions for an airfoil penetrating
into a sharp-edged vertical gust
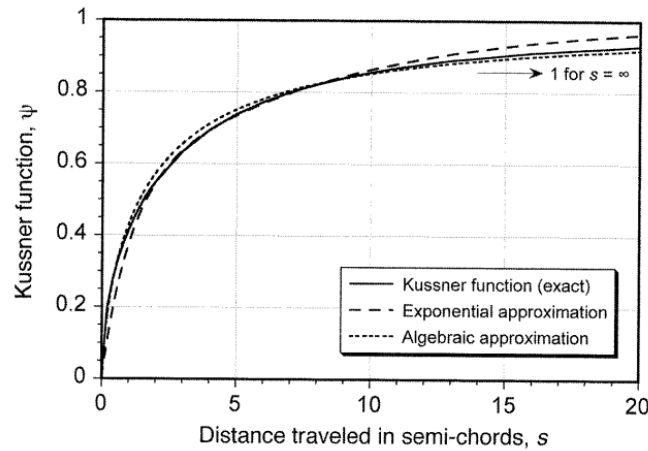
(b) Küssner's function for the penetration of a
sharp-edged vertical gust

Figure 2.14: Küssner's function (Ref. [Küs36])

2.4 State-Space Model

Here the *state* describes the internal behavior of that system and is simply the information required at a given instant in time to allow the determination of the outputs from the system given future input. Variables that form a

state describe the internal mechanics of the system, and they are called state variables; for example, following Ziemer Ref. [ZTF84] a general nth order differential system with m inputs and p outputs may be represented by n first-order differential equations.

Simple differential equations can represent dynamic systems because they have properties about how a system is changing at any given time as a function of its current state. The state-space model helps define stability for linear systems with the help of the state and its derivative; if energy dissipates over time, then the system is stable, and if energy dissipates faster, then the system is more stable. If the energy is growing unboundedly, then the system is unstable.

$$\underbrace{\underbrace{\dot{x}}_{\text{derivatives}} = \underbrace{f(x,u)}_{\text{states and external inputs}}}_{\text{defines how a system changes}} \tag{2.26}$$

State-space representation repackages the higher order differential equations to first order ODE. The repackaging of the higher order equations to first order equations helps in understanding how the change of state related to its current state and how external input affects it, as shown in equation **??** and 2.26. The state-space model has been used in building many control techniques such as Kalman filter control, LQR control, robust control, and model predictive control, to name a few. Derivative of the system states can be found by linear combinations of the current states plus linear combinations of external inputs. This formulation helps avoid the entire dynamic of the system and only focuses on state relations.

$$\begin{aligned} state \ equation \Longrightarrow \dot{x}(t) = Ax(t) + Bu(t) \\ output \ equation \Longrightarrow y(t) = Cx(t) + Du(t) \end{aligned} \tag{2.27}$$

2.5 VAST

VAST (Versatile Aeromechanics Simulation Tool) is a new multi-physics simulation environment for the highly complex field of helicopter comprehensive analysis. Researchers developed it from the German Aerospace Research Center (DLR) - Institute of Flight Systems Technology in the frame of the DLR Project Victoria. VAST uses a general state-space approach for the physics model and a multi-body approach for structural mechanics. The implemented models for aerodynamics include unsteady aerodynamics based

on a semi-empirical analytical model for the blade sectional airloads and a vortex-lattice model for the computation of the rotor wake (Ref. [Hof+20]). The principal idea is coupled system of models that are expressed as a state-space model as shown in figure 2.17 (a) and figure 2.15 shows the main component of VAST with typical workflow from left to right.

VAST simulation framework can be divided into four parts as shown in figure 2.16. The first one is *initialization* module, which handles the configuration of the model to simulate. Followed by the *core*, it performs the non-linear time simulation (Ref. 2.16). The *system analysis* helps in the analysis of trim or eigenanalysis. Overall, the *process control* module essentially executes a list of tasks for the calculation.
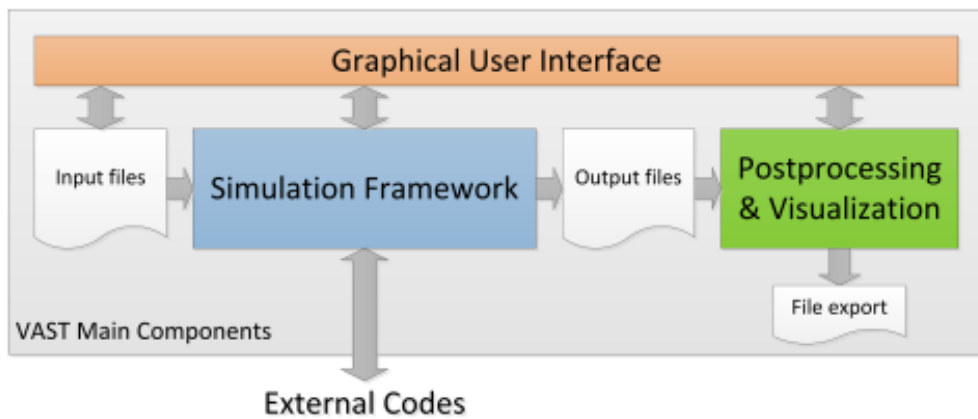
Figure 2.15: Main component of VAST (Ref. [Hof+20])
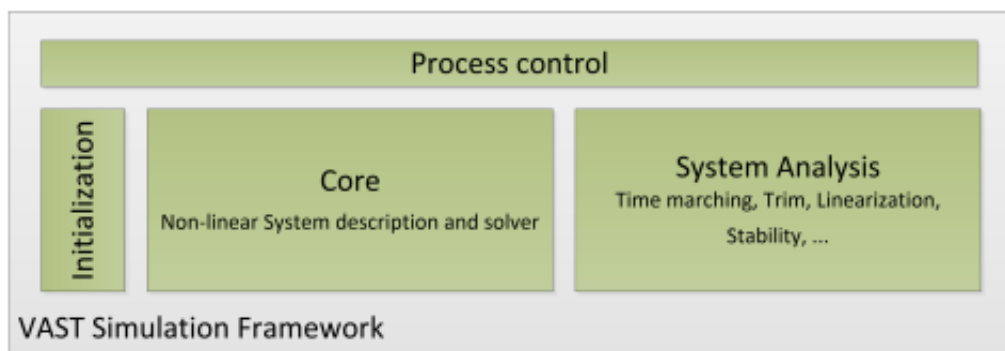
Figure 2.16: VAST simulation frame (Ref. [Hof+20])

(a) Generic State-Space Model

(b) The VAST solver
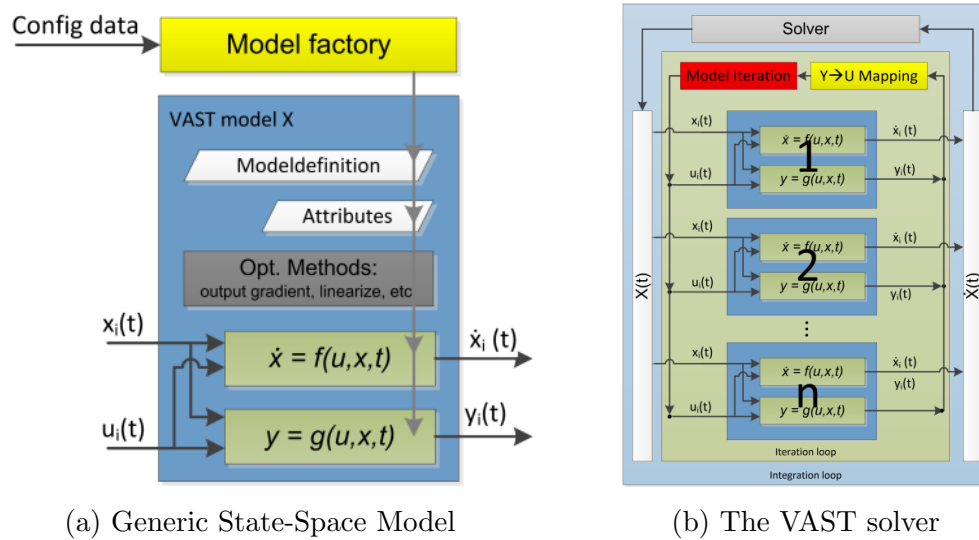
Figure 2.17: The VAST (Ref. [Hof+20])

3 Model Implementation

This chapter will provide an overview of the model implementation adopted in this work. It starts with a brief overview of indicial response function formulation, followed by the description of the state-space model for attached flow and dynamic stall effects. Finally, the modification adopted from Leishman and Beddoes for the reattachment of flow.

3.1 General Indicial Response

In reality, helicopter blades encounter arbitrary motion, and hence we need to find the aerodynamic response for it. Indicial aerodynamic response(s) helps find unsteady aerodynamic forces and pitching moments in the time domain in response to arbitrary AoA and/or inflow velocity using the Duhamel superposition. Wagner's model, as discussed in 2.3.2 is an indicial response function.

An indicial response function is the response to the disturbance applied instantaneously at instant time zero and held constant after that. Examples are an airfoil experiencing a sudden change in AoA and/or airfoil entering the sharp edge gust. There are two challenges of this method. The first is to find the approximate indicial response function for compressible flow. The second is to design an efficient numerical method that provides accuracy and is computationally efficient in performing the superposition process.

Leishman and Beddoes [LB86] adopted two different approaches to obtain the total indicial response solution: one to solve for the initial loading, which is impulsive and decays rapidly with time, and another for the circulatory loading, which builds up quickly in the first few chord length travels and tend asymptotically to the appropriate steady-state value. The continuity between initial impulsive loading and succeeding circulatory loading is preserved using linear superposition.

3.1.1 State-Space Equation from Indicial Response

Unsteady aerodynamic response in differential equations or state-space can be directly appended with the structural dynamic equations governing the airfoil or blade motion. This explicit state-space formulation enables stability analysis for rotor blades based on eigenvalue analysis.

In the VAST model case, the inputs u to the system are the AoA and pitch rate, and the outputs y are the required lift force, chord force, and pitching moment. State-space formulation describing the unsteady aerodynamics can

be obtained by applying the Laplace transform to the indicial response function from equation 2.12. A general form of the aerodynamic state-equation is as follows:

$$\mathcal{L}[h(t)] = \frac{(A_1 b_1 + A_2 b_2)(\frac{2V}{c})p + (b_1 b_2)(\frac{2V}{c})^2}{p^2 + (b_1 + b_2)(\frac{2V}{c})p + (b_1 b_2)(\frac{2V}{c})^2} \tag{3.1}$$

Input $\longrightarrow$ | Laplace transfer function $\mathcal{L}[h(t)]$ | $\longrightarrow$ output
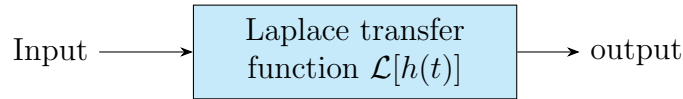
Figure 3.1: Flowchart for indicial response to state space model

$$\begin{bmatrix} \dot{x}_1 \\ \dot{x}_2 \end{bmatrix} = \left(\frac{2V}{c}\right) \begin{bmatrix} -b_1 & 0 \\ 0 & -b_2 \end{bmatrix} \begin{bmatrix} x_1 \\ x_2 \end{bmatrix} + \begin{bmatrix} 1 \\ 1 \end{bmatrix} \alpha(t) \tag{3.2}$$

$$C_N(t) = C_{l\alpha} \left(\frac{2V}{c}\right) \begin{bmatrix} A_1 b_1 & A_2 b_2 \end{bmatrix} \begin{bmatrix} x_1 \\ x_2 \end{bmatrix} \tag{3.3}$$

These equations are in the form of equation **??** and this case, matrix D is equal to zero. Hence we need to find the correct indicial response function to get the state-space form.

Tran Ref. [TP80] was the first to adopt the state-space form to describe the unsteady aerodynamic response of a 2D airfoil. However, Tran got reasonable success, but air load quantitative prediction capability can be improved further. For general application to a variety of airfoil sections, a model must meet the following conditions; the First one is well-proven classical unsteady aerodynamic methods for *attached flows* and can be used to estimate the *dynamic stall* characteristics from the static stall characteristics, and it must also include the modeling of key factors *leading edge separation (LES) and trailing edge separation (TES) together with leading-edge vortex shedding.*

3.2 Leishmann-Crouse State-Space Attached Flow Model

Leishman and Crouse adopted "Airfoil Unsteady Aerodynamic Behaviour and Dynamic Stall, using the Indicial Method" Ref. [LB86] by Leishman and Beddoes for the development of the state-space model for the unsteady dynamic stall. Leishman and Crouse presented the state-space formulation for attached flow in Ref. [LC89] and dynamic stall in Ref [Lei89]. The

VAST model is developed based on state-space formulation from Leishman and Crouse, with the model modifications adopted from the Leishman and Beddoes [LB86].

The VAST model is divided into four subsystems as shown in Figure 3.2: unsteady attached flow, trailing edge flow separation, leading-edge flow separation, and vortex shedding. However, we do not have a model to capture the complex viscous effects; hence it is avoided by using empirically derived time constant from unsteady, 2D oscillating, or plunging wind tunnel experiments. Therefore, only 2D effects on an airfoil cross-section are considered.
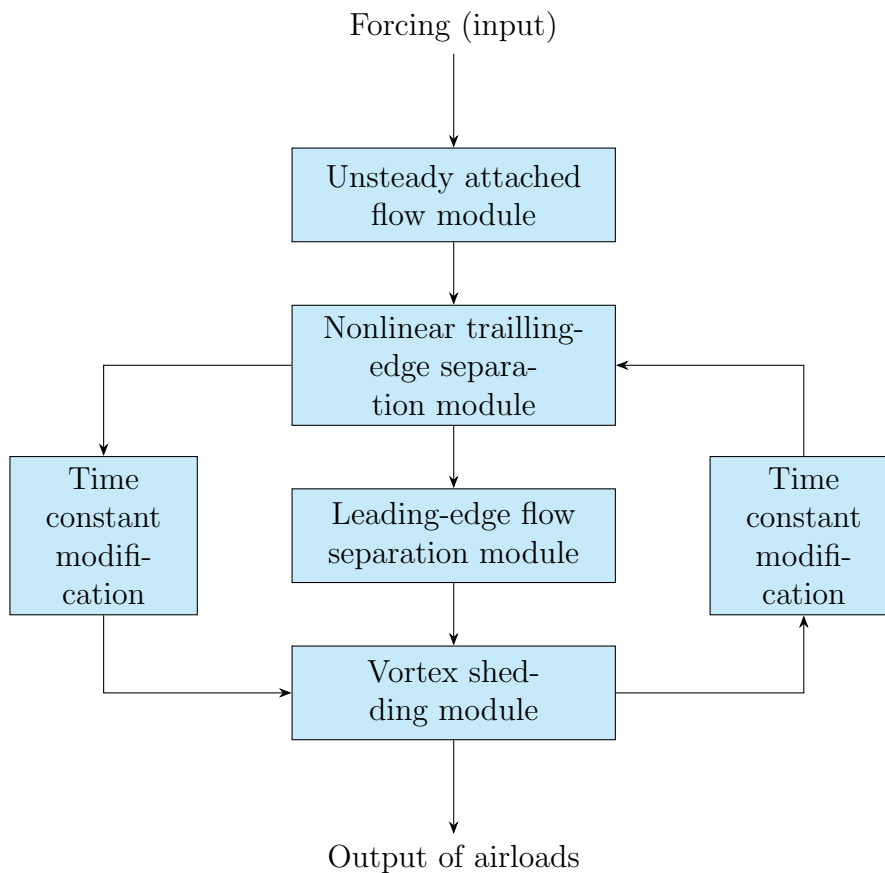
Figure 3.2: Flowchart for Leishmann-Beddoes Unsteady Airfoil Behaviour and Dynamic Stall

3.2.1   Unsteady Attached Flow Behavior

A prerequisite in any unsteady aerodynamic theory is accurately representing the unsteady aerodynamic response under attached flow conditions. Beddoes

Ref. [Bed82] considered a non-circulatory lift component due to impulsive loading from the added mass term, which decays exponentially with distance traveled. The Circulatory lift component, which develops as distance traveled by airfoil and asymptotically attains a value of steady-state and it corresponds to the bound vortex lift as shown in 3.3.

(a) Normal force response

(b) Moment response
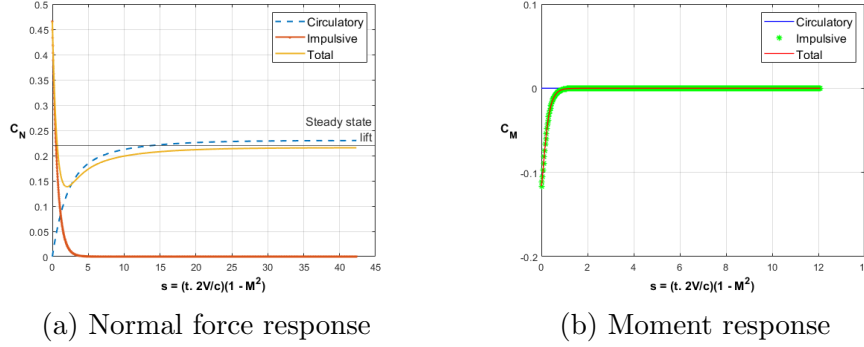
Figure 3.3: VAST total inidicial response for step change in the AoA at $\Delta\alpha = 2°$ and M=0.3

According to Leishman and Beddoes, the analytical indicial response function is only available for the incompressible flow. However, for subsonic compressible flow, there is no convenient analytic equivalent. Because subsonic flow is hyperbolic and incompressible flow is elliptic in nature. With the help of Piston theory, we can find the initial loading on the airfoil after step input which results in the compression wave on the upper surface of the airfoil and expansion wave on the lower surface of the airfoil. By taking a pressure difference on a single airfoil element and then integrating the exact chordwise pressure, we can get an analytical solution for the normal force and pitching moment component.

In subsonic flow, decomposition of the total loading in circulatory and non-circulatory parts is just for idealization because it is convenient for handling the problem. The approximate form of the normal force and pitching moment coefficient for circulatory and non-circulatory loading for subsonic compressible flow are as follow:

$$C_{N\alpha}(S) = \left[\frac{4}{M}\phi_\alpha^I(S) + \frac{2\pi}{\beta}\phi_\alpha^C(S) \right] \tag{3.4}$$

$$C_{M\alpha}(S) = \left[\frac{-1}{M}\phi_{\alpha M}^I(S) - \frac{2\pi}{\beta}\phi_\alpha^C(S)\left[x_{ac}(M) - 0.25\right] \right] \alpha \tag{3.5}$$

$$C_{Nq}(S) = \left[\frac{-1}{M} \phi_q^I(S) - \frac{\pi}{\beta} \phi_q^C(S) \right] q \tag{3.6}$$

$$C_{Mq}(S) = \left[\frac{-7}{12M} \phi_{qM}^I(S) + \frac{-\pi}{8\beta} \phi_{qM}^C(S) \right] q \tag{3.7}$$

$C_{N\alpha}(S)$ represents normal force coefficient due to step change in AoA, $C_{M\alpha}(S)$ represents pitching moment coefficient due to step change in AoA, $C_{Nq}(S)$ represents normal force coefficient due to step change in pitching rate, $C_{Mq}(S)$ represents pitching moment coefficient due to step change in pitching rate, M is the local mach number, ϕ_α^I non-circulatory indicial response function for the step change in AoA, ϕ_α^C circulatory indicial response function for the step change in AoA, $\phi_{\alpha M}^I$ non-circulatory indicial response function for the step change in AoA and pitch rate, ϕ_q^I non-circulatory indicial response function for the step change in pitch rate, ϕ_q^C circulatory indicial response function for the step change in pitch rate, and $\phi_{\alpha M}^C$ circulatory indicial response function for the step change in AoA and pitch rate.

Coefficients of $\phi_c(S)$ have been selected based on experimental and theoretical analysis where exponential functions are scaled by β^2, and it has been documented by Beddoes [Bed82].

The total normal force coefficient for attached flow as shown in equation 3.18 and respective circulatory and non circulatory indicial response functions with corresponding state space form are as follow

$$\phi_\alpha^C(S) = 1.0 - A_1 \exp\left(-b_1 \beta^2 S\right) - A_2 \exp\left(-b_2 \beta^2 S\right)$$

$$\begin{bmatrix} \dot{x}_1 \\ \dot{x}_2 \end{bmatrix} = \left(\frac{2V}{C} \right) \beta^2 \begin{bmatrix} -b_1 & 0 \\ 0 & -b_2 \end{bmatrix} \begin{bmatrix} x_1 \\ x_2 \end{bmatrix} + \begin{bmatrix} 1 \\ 1 \end{bmatrix} \alpha_{3/4}(t) \tag{3.8}$$

$$C_N^C(t) = \frac{2\pi}{\beta} \left(\frac{2V}{c} \right) \beta^2 \begin{bmatrix} A_1 b_1 & A_2 b_2 \end{bmatrix} \begin{bmatrix} x_1 \\ x_2 \end{bmatrix} \tag{3.9}$$

$$\phi_\alpha^I(S) = \exp\left(\frac{-S}{T_\alpha} \right) \tag{3.10}$$

$$K_\alpha(M) = \left[\frac{1}{(1 - M) + \pi \beta M^2 (A_1 b_1 + A2 b_2)} \right] \tag{3.11}$$

$$\dot{x}_3 = \alpha(t) - \frac{1}{K_\alpha T_I} x_3 \tag{3.12}$$

$$C_{N\alpha}^I = \frac{4}{M} \dot{x}_3 \tag{3.13}$$

$$\phi_q^I(S) = \exp\left(\frac{-S}{T_q}\right) \tag{3.14}$$

$$K_q(M) = \left[\frac{1}{(1 - M) + 2\pi\beta M^2 (A_1 b_1 + A2b_2)}\right] \tag{3.15}$$

$$\dot{x}_4 = q(t) - \frac{1}{K_q T_I} x_4 \tag{3.16}$$

$$C_{Nq}^I = \frac{1}{M} \dot{x}_4 \tag{3.17}$$

$$C_N^P(t) = C_N^C(t) + C_{N\alpha}^I(t) + C_{Nq}^I(t) \tag{3.18}$$

$$A_1 = 0.3, A_2 = 0.7, b_1 = 0.14, b_2 = 0.53$$

The circulatory and non-circulatory indicial response functions with a corresponding state-space form for the pitching moment are as follow:

$$\phi_{\alpha M}^I(S) = A_3 \exp\frac{-S}{b_3 T_{\alpha M}} + A_4 \exp\frac{-S}{b_4 T_{\alpha M}}$$
$$K_{\alpha M}(M) = \left[\frac{A_3 b_4 + A_4 b_3}{b_3 b_4 (1 - M)}\right] \tag{3.19}$$

$$\begin{bmatrix} \dot{x}_5 \\ \dot{x}_6 \end{bmatrix} = \begin{bmatrix} a_{55} & 0 \\ 0 & a_{66} \end{bmatrix} \begin{bmatrix} x_5 \\ x_6 \end{bmatrix} + \begin{bmatrix} 1 \\ 1 \end{bmatrix} \alpha(t)$$
$$C_{M\alpha}^I(t) = \frac{-1}{M} \begin{bmatrix} A_3 a_{55} & A_4 a_{66} \end{bmatrix} \begin{bmatrix} x_5 \\ x_6 \end{bmatrix} - \frac{1}{M} \alpha(t) \tag{3.20}$$

$$where \quad a_{55} = -\frac{1}{(b_3 K_\alpha M T_I)} \quad a_{66} = -\frac{1}{(b_4 K_\alpha M T_I)}$$

$$\phi_{qM}^C(S) = 1 - \exp\left(-b_5\beta^2 S\right)$$

$$\phi_{qM}^I(S) = \exp\frac{-S}{T_{qM}}$$

$$\phi_{qM}^I(t) = \exp\frac{-t}{K_{qM}T_I} \tag{3.21}$$

$$K_{qM}(M) = \left[\frac{7}{15(1-M) + 3\pi\beta M^2 b_5}\right]$$

$$\dot{x}_7 = q(t) - b_5\beta^2\left(\frac{2V}{c}\right)x_7 = q(t) + a_{77}x_7$$

$$\dot{x}_8 = q(t) - \left(\frac{1}{K_{qM}T_I}\right)x_8 = q(t) + a_{88}x_8 \tag{3.22}$$

$$C_{Mq}^C(t) = -\frac{\pi}{8\beta}b_5\beta^2\left(\frac{2V}{c}\right)x_7$$

$$C_{Mq}^I(t) = -\frac{7}{12M}\dot{x}_8 \tag{3.23}$$

$$C_M^P(t) = C_{Mq}^C(t) + C_{M\alpha}^I(t) + C_{Mq}^I(t) \tag{3.24}$$

$$A_3 = 1.5, A_4 = 0.5, b_3 = 0.25, b_4 = 0.1, b_5 = 0.5$$

Coefficients of $\phi_{\alpha M}(S)$ have been selected based on comparing the response with the exact linear theory results of Lomax Ref. [Lom+52] and with Bisplinghoff Ref. [BAH13].

Leishman obtained the non-circulatory time constant $K_\alpha(M), K_q(M), K_{\alpha M}(M)$ and $K_{qM}(M)$ in Ref. [Lei88]. The exact linear theory results of Lomax Ref. [Lom+52] can be used to estimate the time constants by matching the gradient of the total response for S=0 where $T_I = c/a$. [Lom+52].

The overall unsteady aerodynamic response can be shown in figure 3.4. It can be readily shown that by grouping the state equations previously derived, they can be represented in the general form by Leishman [LC89].

$$a_{11} = -\left(\frac{2V}{c}\right)\beta^2 b_1; a_{22} = -\left(\frac{2V}{c}\right)\beta^2 b_2; a_{33} = -\frac{1}{K_\alpha T_I}; a_{44} = -\frac{1}{K_q T_I};$$
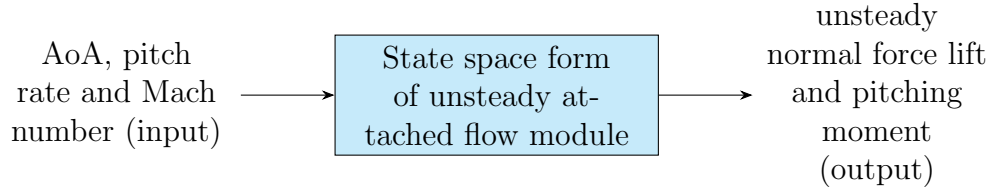
Figure 3.4: Flowchart unsteady attached flow

$$c_{11} = -\frac{2\pi}{\beta}\left(\frac{2V}{c}\right)\beta^2 A_1 b_1 x_1 ; c_{12} = -\frac{2\pi}{\beta}\left(\frac{2V}{c}\right)\beta^2 A_2 b_2 x_2 ; c_{13} = -\frac{4}{M}\left(\frac{1}{K_\alpha T_I}\right);$$

$$c_{14} = -\frac{1}{M}\left(\frac{1}{K_q T_I}\right); c_{25} = -\frac{1}{M}\left(\frac{A_3}{b_3 K_{\alpha m} T_I}\right); c_{26} = -\frac{1}{M}\left(\frac{A_4}{b_4 K_{\alpha m} T_I}\right);$$

$$c_{27} = -\frac{\pi}{16}\left(\frac{2V}{c}\beta\right); c_{28} = -\frac{7}{12M}\left(\frac{1}{K_{qm} T_I}\right);$$

$$\begin{Bmatrix}\dot{x}_1\\\dot{x}_2\\\dot{x}_3\\\dot{x}_4\\\dot{x}_5\\\dot{x}_6\\\dot{x}_7\\\dot{x}_8\end{Bmatrix} = \begin{bmatrix}a_{11} & 0 & 0 & 0 & 0 & 0 & 0 & 0\\0 & a_{22} & 0 & 0 & 0 & 0 & 0 & 0\\0 & 0 & a_{33} & 0 & 0 & 0 & 0 & 0\\0 & 0 & 0 & a_{44} & 0 & 0 & 0 & 0\\0 & 0 & 0 & 0 & a_{55} & 0 & 0 & 0\\0 & 0 & 0 & 0 & 0 & a_{66} & 0 & 0\\0 & 0 & 0 & 0 & 0 & 0 & a_{77} & 0\\0 & 0 & 0 & 0 & 0 & 0 & 0 & a_{88}\end{bmatrix}\begin{bmatrix}x_1\\x_2\\x_3\\x_4\\x_5\\x_6\\x_7\\x_8\end{bmatrix} + \begin{bmatrix}1 & 0.5\\1 & 0.5\\1 & 0\\0 & 1\\1 & 0\\1 & 0\\0 & 1\\0 & 1\end{bmatrix}\begin{Bmatrix}\alpha\\q\end{Bmatrix}$$

$$\begin{Bmatrix}C_N\\C_M\end{Bmatrix} = \begin{bmatrix}c_{11} & c_{12} & c_{13} & c_{14} & 0 & 0 & 0 & 0\\c_{21} & c_{22} & 0 & 0 & c_{25} & c_{26} & c_{27} & c_{28}\end{bmatrix}\begin{Bmatrix}x_1\\x_2\\x_3\\x_4\\x_5\\x_6\\x_7\\x_8\end{Bmatrix} +$$

$$\begin{bmatrix}4/M & 1/M\\-1/M & -7/12M\end{bmatrix}\begin{Bmatrix}\alpha\\q\end{Bmatrix}$$

3.3 Leishmann-Crouse State-Space Dynamic Stall Model

3.3.1 Extension to the Non-linear Regime

The earlier section established a state-space governing equation for attached flow (linearized) airfoil behavior. In this section, we will be focusing on the formulation of the state-space model for the non-linear airfoil behavior and dynamic stall.

The airfoil non-linear aerodynamics behavior in the Mach number range of interest is due to viscous effects and viscous-inviscid interactions. Therefore, a generalized aerodynamic model for non-linear behavior must allow for the progressive effects of trailing edge separation (TES) and abrupt effects of leading-edge separation (LES) or shock-induced separation.

3.3.2 Stall Onset

The onset of LES occurs when the leading edge encounters the critical pressure and associated pressure gradient. Evans and Mort [EM59] came up with the equivalent criteria with the help of static airfoil data to capture the onset of stall. Beddoes [Bed78] evaluated Evans and Mort's criteria under both steady and unsteady conditions. As per Beddoes, Evans and Mort's criteria have performed well in capturing the onset of the stall by considering local leading-edge velocity as the primary factor. Later Beddoes [Bed83] used the same criteria to extend the model for higher Mach number to capture the onset of shock-induced stall. In application, pressure (P) is related to the C_N, and hence we can use the critical value of C_N at the onset of the stall, which can be found from static airfoil test data. From the analysis of airfoil static test data for various Mach numbers critical value of $C_N(\text{static}) = C_{N_1}$ a stalled boundary can be defined as shown in figure 3.5 for the NACA0012 airfoil.

From dynamic tests Leishman found that, there is a phase lag of the airfoil peak pressures under nominally attached flow conditions for the instantaneous normal lift force. In the case of unsteady flow, aerodynamic responses experience lag due to temporal effects. The pressure distribution and coefficient of lift are achieved at a higher AoA than intended. Which will result in an overall delay in the dynamic stall. Hence, a first-order lag may be applied to $C_N(t)$ to produce a substitute value $C_N'(t)$ with the presumption that whatever properties apply to $P(t)$ must also apply to $C_N'(t)$. From tests over the relevant Mach number range, it is found that pressure phase lag is nominally linear within the interested Mach number range and increases with an increase in Mach number. The first-order lag with Mach number
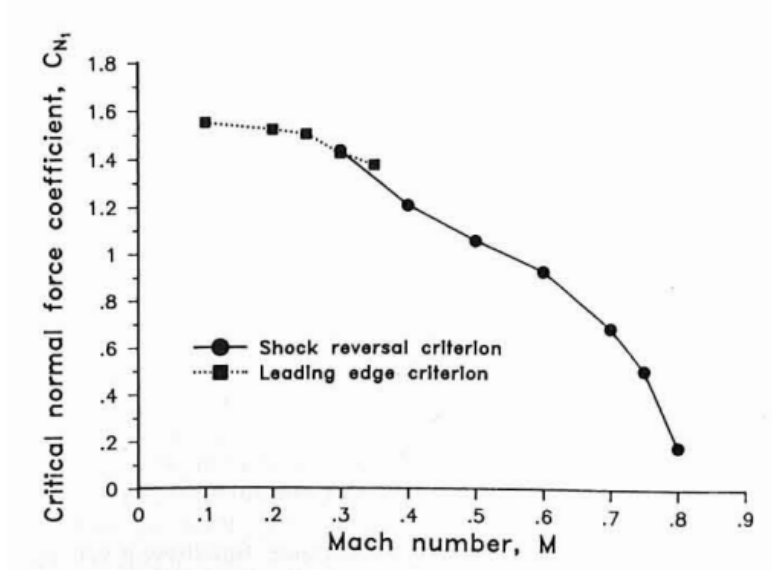
Figure 3.5: Critical normal force separation onset boundary or stall boundary for the NACA-0012 airfoil (Ref. [LB86])

dependent time constant T_p can be applied to static relation for normal force coefficient in attached flow condition C_N^P which gives a coefficient of normal lift C_N'. State-space form to obtain the $C_N'(t)$ is represented as follows

$$\dot{x}_9 = -\frac{x_9}{T_p} + \frac{C_N^P(t)}{T_p}$$

$$C_N'(t) = x_9$$

(3.25)

Where the input to the equation 3.25 is the total unsteady lift under attached flow condition $C_N^P(t)$ and the time constant for leading edge pressure response T_p. The time constant T_p is a function of Mach number and can be determined empirically from unsteady airfoil data. The value of T_p is largely independent of airfoil shape. Once $C_N'(t)$ exceeds C_{N_1} the onset of leading edge/shock induced separation under dynamic conditions will be initiated and when $C_N'(t) < C_{N_1}$ flow reattaches to airfoil under dynamic flow condition.

3.3.3 Trailing Edge Separation

As an airfoil undergoes a stall, a trailing edge flow separation occurs, and the separation point progresses toward the leading edge. The airfoil loses the circulation associated with it, and the aerodynamic response of airfoil

shows non-linearities in force and moment behavior. Hence capturing the TES and its effect on aerodynamic response becomes crucial. Wilby [Wil84] findings show that trailing edge separation may play a vital role in the onset of dynamic stall. Wilby also shows that the moderate pitch rate can suppress trailing edge separation. However, studies have shown that this will leads to abrupt leading-edge separation or shock-induced flow separation if the supercritical flow is allowed to develop. Even when the primary source of separation is at the airfoil leading edge or a shock wave, it promotes the trailing edge separation through the thickening of the boundary layer.

Kirchhoff presented a theory for separated flow regions on 2D bodies and it was reviewed by Wood in [Woo11]. A specific case is a flow separation on a 2D plate as shown in figure 3.6. The normal force coefficient is given by equation 3.26. Where 2π shows the normal force curve slope for incompressible flow, f is the trailing edge flow separation point, and α is AoA. We can extend this form to get a normal force coefficient for compressible flow as shown in equation 3.27 by replacing the force curve slope 2π with force curve slope $C_{N_\alpha}(M)$ or $(2\pi/\beta)$ at appropriate Mach number which can be obtained through static airfoil data.

$$x/C = f$$

$$V$$
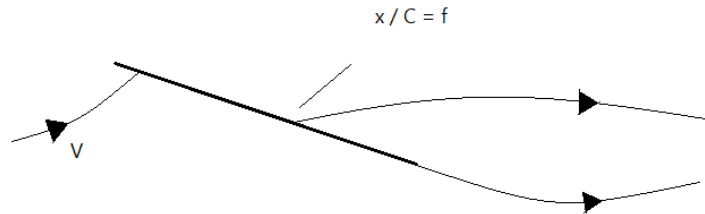
Figure 3.6: Kirchoff flow idealisation

$$C_N = 2\pi \left(\frac{1 + \sqrt{f}}{2} \right)^2 \alpha \tag{3.26}$$

$$C_N = C_{N_\alpha}(M) \left(\frac{1 + \sqrt{f}}{2} \right)^2 \alpha \tag{3.27}$$

An empirical relationship between effective separation point f and AoA α can be obtained by using the static airfoil data as shown in the equation.
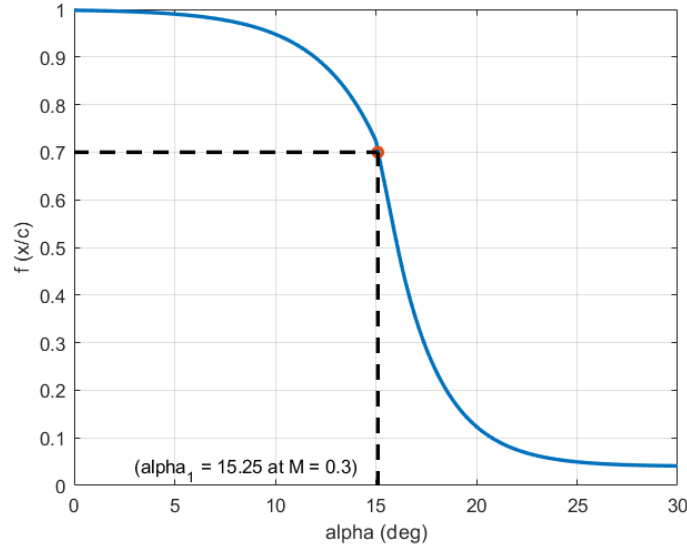
Figure 3.7: Modelling of trailing edge separation point

$$f = \begin{cases} 1 - 0.3 \exp\left\{(\alpha - \alpha_1)/S_1\right\}, & \text{if } \alpha < \alpha_1 \\ 0.04 + 0.66 \exp\left\{(\alpha_1 - \alpha)/S_2\right\}, & \text{if } \alpha > \alpha_1 \end{cases} \tag{3.28}$$

The coefficients S_1 and S_2 define the stall characteristics, while α_1 defines the break point corresponds to $f = 0.7$. For most airfoil section static stall occurs normally at separation point $f \approx 0.7$. S_1, S_2 and α_1 are determined empirically for each airfoil and vary with Mach number as shown in Table 4.5. Figure 3.7 shows the variation of f with AoA for equation 3.28.

Kirchhoff's theory does not provide a generalized formulation for the pitching moment. However, the center of pressure can be found from static airfoil data by the ratio of C_M/C_N. Furthermore, the variation can be plotted versus the separation point, and by using the least square method, a relation between COP and f can be obtained.

$$\frac{C_M}{C_N} = [K_0 + K_1(1 - f) + K_2 sin(\pi f^m)] \tag{3.29}$$

Where K_0, K_1, K_2 and m can be adjusted for different airfoil and $K_0 = (0.25 - X_{ac})$ is the aerodynamic center offset from the $1/4-$ chord. The constant K_1 directly affects the center of pressure due to the growth of the separated flow region, and the constant K_2 helps describe the shape of the moment break

stall. Normally $m = 2$, and it is independent of the type of airfoil. Kirchhoff also gives a generalized expression for chord force for the separated flow. However, in reality, there exists a viscous boundary layer hence chord force will not be completely realized as in the case of potential flow. Therefore, a factor η is used to account for the viscous effect, and $\eta = 100\%$ in the case of potential flow, and for unsteady separated flow from static airfoil data, it has been found that $\eta = 97\%$.

$$C_C = \eta C_{N_\alpha} \alpha^2 \sqrt{f} \tag{3.30}$$

As in the case of temporal effects on airfoil pressure distribution, the boundary layer is also time-dependent. Scruggs Ref. [SNS74] presented a finite difference scheme to integrate boundary layer equations, which were coupled to an unsteady potential flow analysis for a steadily pitching airfoil. Leishman and Beddoes [LB86] presented a simple open-loop procedure to show the time-dependent variation of trailing edge separation point f. Unsteady leading-edge pressure for a quasi-steady case can be found with the help of effective AoA (α_f). The additional effects of the unsteady boundary layer response may be represented by applying a first-order lag to the value of f' to produce the final value for the unsteady trailing edge separation point f''.

$$\alpha_f(t) = \frac{C'_N(t)}{C_{N_\alpha}(M)} \tag{3.31}$$

$$f' = \begin{cases} 1 - 0.3 \exp\left\{(\alpha_f(t) - \alpha_1)/S_1\right\}, & \text{if } \alpha_f(t) < \alpha_1 \\ 0.04 + 0.66 \exp\left\{(\alpha_1 - \alpha_f(t))/S_2\right\}, & \text{if } \alpha_f(t) > \alpha_1 \end{cases} \tag{3.32}$$

The state space form for the f'' can be represented as follow:

$$\dot{x}_{10} = -\frac{x_{10}}{T_f} + \frac{f'(t)}{T_f}$$
$$f''(t) = x_{10} \tag{3.33}$$

The state equation for separation point movement on the airfoil is requires modification of the time constant parameter depending on the physical phenomenon on the airfoil. According to Leishman and Beddoes, the separation point moves faster towards the leading edge during the vortex shedding. On

the other hand, if flow reattachment occurs during the presence of the vortex, then it moves slowly towards the leading edge. So, each time depending on the physical process time constant parameter (T_f) needs to be changed. Therefore, the VAST model adopts the following modifications for *time constant for separation point movement* suggested by Leishman and Beddoes [LB86].

The first one is during the vortex shedding process, the pressure changes occurring are sufficient to accelerate the forward progression of any trailing edge separation, which may be accomplished by halving the instantaneous effective time constant, T_f; in addition, the vortex should not cross the trailing edge. Second, if the direction of pitching motion is changed during the vortex travel, the separation point moves faster towards the leading edge. It can be accomplished by halving the instantaneous effective time constant, T_f. Finally, during the vortex presence the establishment of flow reattachment is delayed considerably until the vortex reaches downstream $(\tau_v > 2 * T_{vl})$. For example, flow reattachment during the onset of stall can be accomplished by considering the instantaneous effective time constant four times, $T_f = 4 * T_f$.

The normal force, pitching moment and chord force coefficient for unsteady flow with trailing edge separation point f'' is given by equation 3.34, 3.35 and 3.36 respectively.

$$C_N^f(t) = C_{N_\alpha}(M) \left(\frac{1 + \sqrt{f''}}{2}\right)^2 \alpha_E(t) \tag{3.34}$$

$$C_M^f(t) = \left[K_0 + K_1(1 - f'') + K_2 sin(\pi(f'')^m)\right] C_N^C + C_{M_0} \tag{3.35}$$

$$C_C^f = \eta C_{N_\alpha} \alpha_E^2 \sqrt{f''} \tag{3.36}$$

After the onset of gross separation, the Kirchhoff modification to the chord force becomes invalid, and an alternative equation with an additional factor is considered by Leishman and Beddoes [LB86], as shown in equation 3.37.

$$C_C(t) = \eta_c C_{N_\alpha} \sin \alpha_E(t) \alpha_E(t) \sqrt{f} \Phi \tag{3.37}$$

$$\Phi = f^{D_f(C_N' - C_{N1})}$$

During the attached flow chord force is calculated from equation 3.36 and during the stall onset equation 3.37. The factor Φ ensures the continuity between the chord force during attached and separated flow. Note that α_E should be in *rad* only in the sin function. Apart from that, it should be in *degree*.

$$C_D = C_N \sin(\alpha) - C_C \cos(\alpha) + C_{D0} \tag{3.38}$$

Separation point with lagged response (f'') is also called dynamic separation point. Dynamic separation point can be used to calculate normal force coefficient, pitching moment coefficient and chord force coefficient as shown in equation 3.34, 3.35, and 3.36 respectively.

However, using the dynamic separation point f'' a satisfactory lift response during the flow reattachment can be obtained, but pitching moment behavior is not acceptable. Because during the flow, reattachment is occasional premature, but localized leading-edge reattachment occurs under some conditions and defers from cycle to cycle. Local leading-edge reattachment may have been due to disturbance in flow fields from interaction effects. For flow reattachment Leishman and Beddoes modeled the pitching moment using the flow separation point from quasi-static flow condition, f_{qs} by considering a moment f-parameter, f_m with time constant half of the T_f.

State equation for the moment modified separation parameter f_m can be represented as shown in equation 3.39. f_{qs}, found using equation 3.28.

$$\dot{x}_{12} = -\frac{2x_{12}}{T_f} + \frac{2f_{qs}(t)}{T_f}$$
$$f_M(t) = x_{12} \tag{3.39}$$

When rate of change of effective incidence is negative, the break angle α_1 is offset by $\delta\alpha_1$.

$$\delta\alpha_1 = (1 - f)^{0.25}\Delta\alpha_1 \tag{3.40}$$

where $\Delta\alpha_1$ is a function of the airfoil and Mach number (Table 4.5). Figure 3.8 shows the variation of f-parameter for deep stall condition with $\alpha = 10° + 10°Sin(\omega t)$; $k = 0.1$ and $M = 0.3$.

3.3.4 Modeling of Dynamic Stall

Unlike trailing edge separation, where the airfoil loses the lift, the leading edge separation caused by vortical disturbances accumulated at the leading
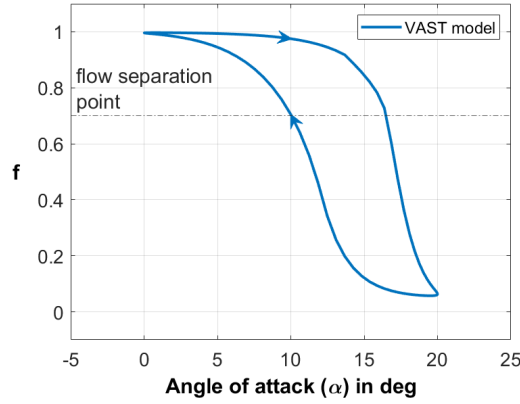
Figure 3.8: Variation of f-parameter for moderate stall condition

edge of the airfoil creates a positive lift before detachment and convecting downstream. These disturbances are small vortices with a negative pressure gradient, increasing the lift on the airfoil. The general case of dynamic stall involves the formation of a vortex at the leading edge of the airfoil; as trailing edge separation progresses, vorticity is shed locally at the separation points and is continuously convected downstream in the shear layer, which results in the pressure gradient being small. Leishman and Beddoes [LB86] formulated a simple but physically acceptable model for the dynamic stall by considering vortex lift contribution $C_N^v(t)$ as excess circulation until a critical condition that $C_N'(t)$ exceeds C_{N_1} is reached. The following state-space equation can represent the circulation produced by a vortex.

$$\dot{x}_{11} = -\frac{x_{11}}{T_v} + \frac{\dot{C}_v}{T_v}$$
$$C_N^v(t) = x_{11}$$

(3.41)

$$C_v = \begin{cases} C_N^C[1 - (1 + \sqrt{f''})^2/4] & for \quad \tau_v \le 2T_{vl} \\ 0 & for \quad \tau_v \le 2T_{vl} \end{cases}$$

(3.42)

State 12 requires the derivative of vortex lift ($\dot{C}_v$) as state input. After inserting the 3.9 into equation 3.42 and differentiating with respect to the time we get quation 3.43.

$$\dot{C}_v = T_1 - (T_1 * T_2 + T_4 * T_3)$$

(3.43)

$$T_1 = K_1 A_1 b_1 \dot{x}_1 + K_1 A_2 b_2 \dot{x}_2$$

$$T_2 = \frac{(1 + f'' + 2\sqrt{f''})}{4}$$

$$T_3 = \dot{x}_{10} + \frac{\dot{x}_{10}}{\sqrt{x_{10}}}$$

$$T_4 = K_1 A_1 b_1 x_1 + K_1 A_2 b_2 x_2$$

$$K_1 = \frac{2\pi}{\beta} \left(\frac{2V}{c} \right) \beta^2$$

$$A_1 = 0.3 \quad A_2 = 0.7$$

$$b_1 = 0.14 \quad b_2 = 0.53$$

When the critical condition is reached, the vortex accumulated at the leading edge of the airfoil starts to convect over the airfoil chord. A new state 13 was formulated to calculate the non-dimensional time τ_v to track the passage of the vortex over the airfoil chord and $\tau_v = 0$ when the vortex detaches from the leading edge during the onset of stall. It is found that the vortex travels with approximately half of the free stream velocity over the chord of the airfoil Ref. [LB86]. During the vortex convection, the lift continues to accumulate through equation 3.41 till it reaches the trailing edge of the airfoil. Once the vortex swept downstream $\tau_v > 2 * T_{vl}$ and τ_v becomes zero until next vortex sheds. The moment produced by the vortex while traveling over the chord is given by the equation 3.44.

$$C_M^v(t) = -CP_v * C_N^v \tag{3.44}$$

$$CP_v(t) = 0.25 * \left[1 - cos \left(\frac{\pi \tau_v}{T_{vl}} \right) \right] \tag{3.45}$$

$$\dot{x}_{13} = \frac{2V}{c}$$
$$\tau_v(t) = x_{13} \tag{3.46}$$

Another additional state is considered to track the direction of pitching moment. When the direction of airfoil changes during the vortex travel the separation point moves much faster towards the airfoil leading edge and for this reason we can use the x_{14}.

$$x_{14} = \dot{\alpha} \tag{3.47}$$

4 Model Validation and Discussion

This section studies the validity of the unsteady dynamic stall model implemented in the VAST. It contains the validation of stall onset, moderate dynamic stall flow, and deep dynamic stall flow.

The unsteady dynamic stall module is evaluated using FORTRAN 90 and implemented in the VAST source code developed by the Institute of Flight System, DLR. The integration of the state equation is performed using the VAST inbuilt solver for solving the coupled ODE, which is based on global fourth-order Runge-Kutta for non-stiff ODEs.

The Unsteady dynamic stall model in VAST is validated against the experimental test, the Leishman-Crouse, and the Leishman-Beddoes state-space model data, from [McC+82], [Lei89], and [LB86] respectively for a NACA-0012 airfoil as shown in Figure. 4.1 under stall onset, moderate dynamic stall, and deep dynamic stall conditions.

The selected data set is for harmonic pitch oscillation at various mean angles of attack with a constant oscillation amplitude of 10° at a reduced frequency (k) of 0.1, and a Mach number of 0.3 set constant for all test cases. All the experimental data presented are ensemble averages of some 25 pitch cycles.
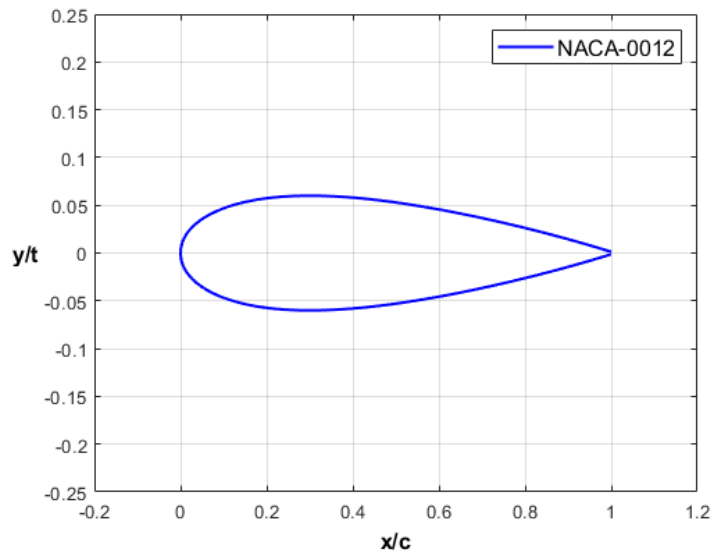

Figure 4.1: NACA-0012 Profile

Parameters	Leishman-Beddoes	Leishman-Crouse
Mach Number, M	0.30	0.30
$C_{L\alpha}$	0.108	0.113
α_1	15.25	14.0
$\Delta\alpha_1$	2.1	-
S_1	3.0	2.75
S_2	2.3	1.4
K_0	0.0025	0.0175
K_1	-0.135	-0.12
K_2	0.04	0.04
C_{D0}	0.0085	-
D_f	8.0	-
C_{N1}	1.45	1.31
T_p	1.7	1.7
T_f	3.0	3.0
T_v	6.0	6.0
T_{vl}	7.0	7.5

Table 4.1: Airfoil coefficients used for unsteady aerodynamic modelling (Ref. [LB86] and [Lei89]).

4.1 Validation of Stall Onset

A NACA-0012 airfoil under harmonic pitch oscillation with amplitude of 10° and reduced frequency $k = 0.1$ and Mach number $M = 0.3$ is considered for stall onset validation. Out of all likely cases of dynamic stall, the onset condition is the most difficult to model because the angle of attack is just sufficient to break the stall boundary condition. Test results from the VAST model are compared with reference data from [Lei89] Fig. 8.

4.1.1 Simulation Configuration

Simulation setup and parameters required in the VAST are as shown in Table 4.2. Airfoil coefficients for state-space model are taken from Table 4.1 for Leishman-Crouse model.

The unsteady dynamic stall state-space model is wholly based on the airfoil coefficients (static airfoil characteristic parameters table 4.5). Therefore, the selection of correct parameters is crucial. Leishman and Beddoes provided an airfoil coefficient table used for unsteady modeling for NACA-0012 for

the range of flight operation envelope. However, Leishman and Beddoes published their findings [LB86] back in 1986. After that, Leishman and Crouse published a state-space representation for unsteady dynamic stall condition Ref. [Lei89]. They adopted different values for the same parameter at the same Mach number as shown in Table 4.1 but only provided data for a single Mach number.

Since, for this test case, the data from Leishman and Crouse are used as a reference for this constant Mach number, we will opt for the airfoil coefficient from Leishman and Crouse over the Leishman and Beddoes table 4.5).

Airfoil section	=	NACA 0012
Blade chord c	=	0.0767 m
Amplitude	=	0.174532925 rad
Amplitude offset	=	0.087266463 rad
Period	=	0.023623545 sec/cycle
Number of cycles	=	25 revolutions
Mach Number	=	0.3
Reduced frequency	=	0.075

Table 4.2: Stall Onset flow configuration

4.1.2 Correlation with Experimental Data and Leishman-Crouse Model

Figure 4.2 shows the normal force, drag force, pitching moment, and chord force coefficient response for a stall onset condition from the VAST model compared with the experimental data and the Leishman-Crouse model response.

The VAST model shows a pretty good correlation with the reference data overall. as shown in Figure 4.2a. The difference in the lift and the lagged lift during the airfoils up and down-stroke, respectively, for the VAST model, is approximately the same as the experimental data, but the Leishman-Crouse model shows large deviations. Specifically, the VAST model correctly predicts the leading-edge stall onset, as shown in figure 4.2a. However, the VAST and Leishman-Crouse models show a lower lift than experimental data during the airfoil down-stroke. Furthermore, the VAST and Leishman-Crouse models show flow reattachment at around AoA of 6.5° and 7.5° respectively, and the experimental data shows flow reattachment at around AoA of 5.7°. In addition, the VAST model shows continuous behavior during the flow reattachment.
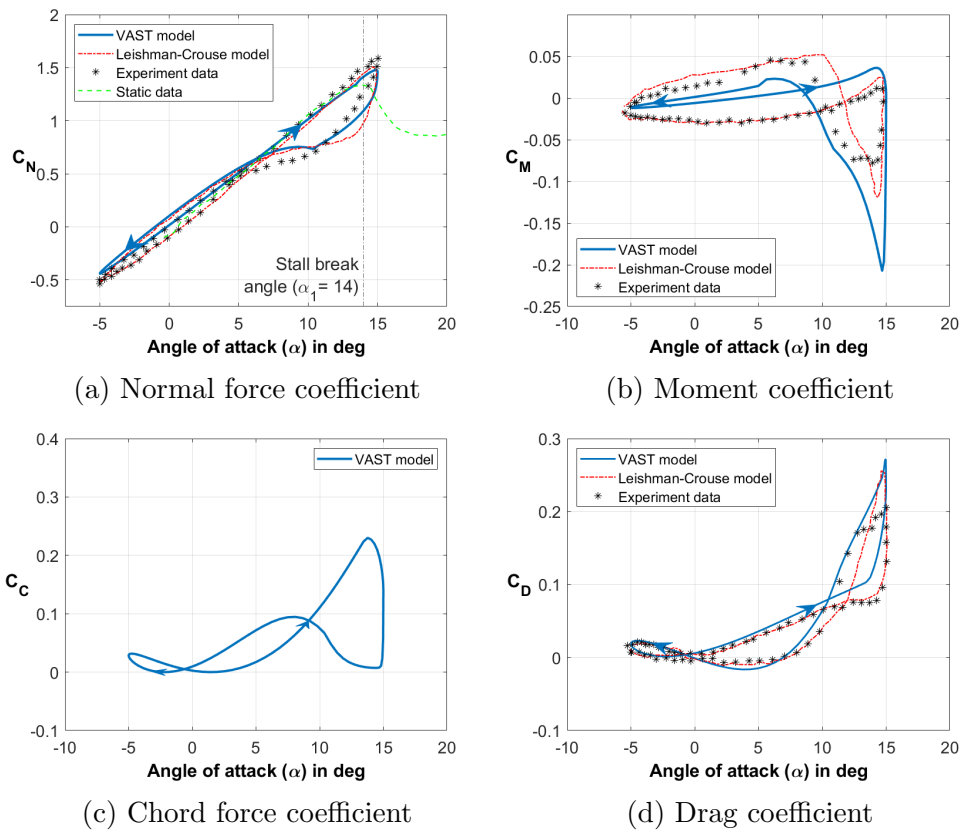
(a) Normal force coefficient

(b) Moment coefficient

(c) Chord force coefficient

(d) Drag coefficient

Figure 4.2: Stall onset $\alpha = 5° + 10° \sin \omega t$; $k = 0.1$ and $M = 0.3$

Figure 4.2b shows the pitching moment coefficient plot. The VAST model qualitatively captures the trend of experiment data and the Leishman-Crouse model response. Specifically, the VAST model captures the small rounded moment break at stall angle. It shows that a small amount of trailing edge flow separation occurs before the onset of the stall. The VAST model shows a better correlation than Leishman-Crouse's model with experimental data after a moment's break. The dynamic flow separation point f is used during the upstroke of the airfoil and a modified separation point f_m based on f_{qs} is used for the flow reattachment. However, the VAST model does not realize the full pitching moment during the up-stroke of the airfoil.

Figure 4.2c shows the chord force coefficient plot. We do not have experimental and Leishman-Crouse model data for chord force validation. Leishman and Crouse also did not discuss the model modification in Ref. [Lei89] for chord force coefficient during the stall onset. However, we can say that the trend of chord force is captured well because chord force is related to the normal force and drag force coefficient, but there might be differences in magnitude.

Figure 4.2d shows the drag coefficient plot, and it shows the strong correlation with the trends of the experimental and Leishman-Crouse models. The deviation in the range 11° to −1° of AoA during the down-stroke of the airfoil may be due to the chord force coefficient. Leishman-Crouse Table 4.1 does not provide any value for drag divergence, which is essential in chord force modification suggested by Leishman and Beddoes. However, presently D_f value is taken from Leishman-Beddoes.

4.2 Validation of Moderate Dynamic Stall

A NACA-0012 airfoil under harmonic pitch oscillation with amplitude of 10°, offset of 10°, reduced frequency $k = 0.1$ and Mach number $M = 0.3$ is considered for moderately strong dynamic stall validation. Under these conditions, leading-edge vortex shedding is initiated, and the characteristic lift overshoot and strong nose-down pitching moment behavior are exhibited. Test results from the VAST model are compared with reference data from [Lei89] Fig. 9.

4.2.1 Simulation Configuration

Simulation setup and parameters required in the VAST are as shown in Table 4.3. Airfoil coefficients for state-space model are taken from Table 4.1 for Leishman-Crouse model.

| Airfoil section	=	NACA 0012
Blade chord c	=	0.0767 m
Amplitude	=	0.174532925 rad
Amplitude Offset	=	0.174532925 rad
Period	=	0.023623545 sec/cycle
Number of cycles	=	25 revolutions
Mach number	=	0.3
Reduced frequency	=	0.1

Table 4.3: Moderate dynamic stall configuration

### 4.2.2 Correlation with Experimental Data and Leishman-Crouse Model

Figure 4.3 shows the normal force, pitching moment, chord force, and drag force response for a moderately strong dynamic stall condition from the VAST model compared with the experimental data and the Leishman-Crouse model (Ref. [Lei89] Fig. 9). The VAST model provides qualitative results for moderate dynamic stall by capturing the normal force coefficients approximately close to experimental and Leishman-Crouse data. In addition, the VAST and the Leishman-Crouse model show the flow reattachment around 5° of AoA, and experimental data shows flow reattachment at 4°, which is captured quite nicely by both models considering the complexity involved in flow reattachment modeling.

Figure 4.3b shows the pitching moment coefficient plot. The VAST model excellently captures the qualitative trend of experimental data and the Leishman-Crouse model response. In addition, The VAST model also shows an excellent rounded moment break at the onset of the dynamic stall; this suggests the presence of trailing edge flow separation before the stall moment break. The Center of pressure variation in the attached flow region is modeled using the dynamic separation point f. The further details regarding the f, f_{qs}, and f_m are given in the section 3.3.3. However, the VAST model over-predicts the pitching moment during the stall break and under-predict during the flow reattachment. Further changes can be made to include the f_m parameter earlier than the stall break to obtain more appropriate coefficients like the experimental data and the Leishman-Crouse model.

Figure 4.3d shows the drag coefficient plot. Again VAST model shows an excellent correlation with the experimental data and the Leishman-Crouse model. The deviations in the drag plots are attributed to the absence of a correct model for chord force modification. The main drag source in a
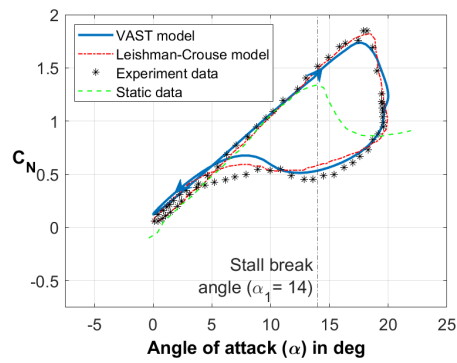
(a) Normal force coefficient
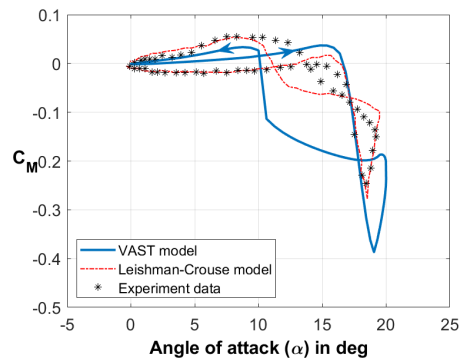
(b) Moment coefficient
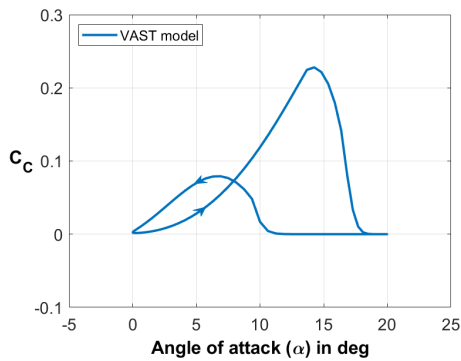
(c) Chord force coefficient

(d) Drag coefficient

Figure 4.3: Moderately strong dynamic stall $\alpha = 10° + 10° \sin \omega t$; $k = 0.1$ and $M = 0.3$

(a) Moderate dynamic stall vortex moment

(b) Moderate dynamic stall vortex lift

Figure 4.4: Moderate dynamic stall vortex shedding

separated flow comes from small and large eddies in a separated flow.

4.3 Validation of Deep Dynamic Stall

A NACA-0012 airfoil under harmonic pitch oscillation with amplitude of 10°, offset of 15°, reduced frequency $k = 0.1$ and Mach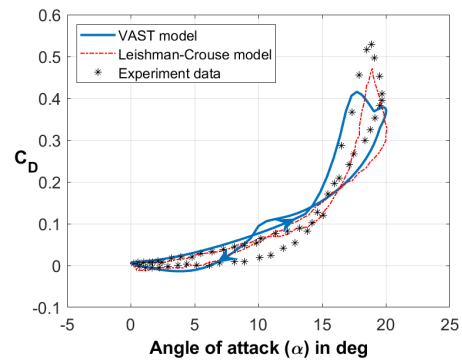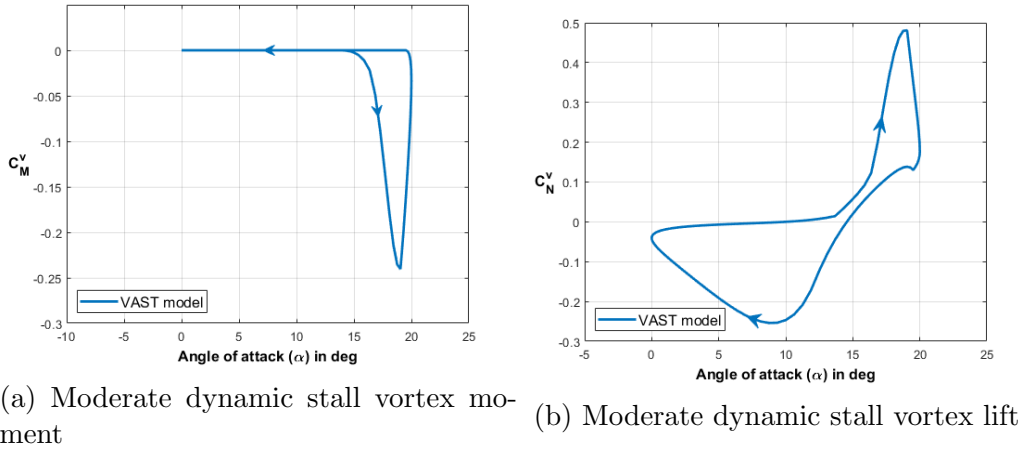 number $M = 0.3$ is considered for deep dynamic stall validation. Under a deep dynamic stall, the airfoil undergoes strong multiple leading-edge vortex sheddings with a significant increase in normal force, pitching moment, and drag. Test results from the VAST model are compared with reference data from [Lei89] Fig. 10.

4.3.1 Simulation Configuration

Simulation setup and parameters required in the VAST are as shown in Table 4.4. Airfoil coefficients for state-space model are taken from Table 4.1 for Leishman-Crouse model.

4.3.2 Correlation with Experimental Data and Leishman-Crouse Model

Figure 4.5 shows the normal force, drag force, pitching moment, and chord force response for a deep dynamic stall condition from the VAST model compared with Ref. [Lei89] Fig. 10. The VAST model follows closely the trend of experimental data and Leishman-Crouse model as shown in Figure 4.5a. However, the VAST model falls short 0.3 of normal force coefficient compared
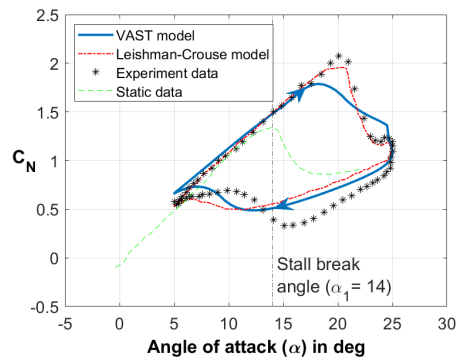
(a) Normal force coefficient
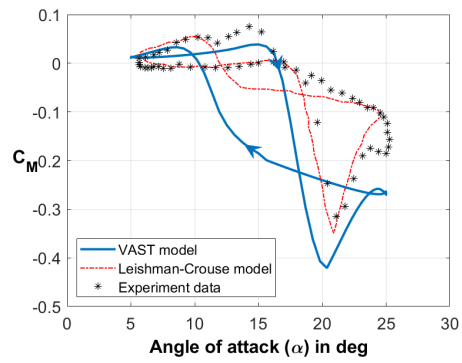
(b) Moment coefficient
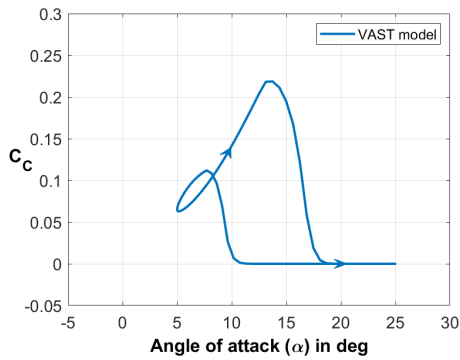
(c) Chord force coefficient
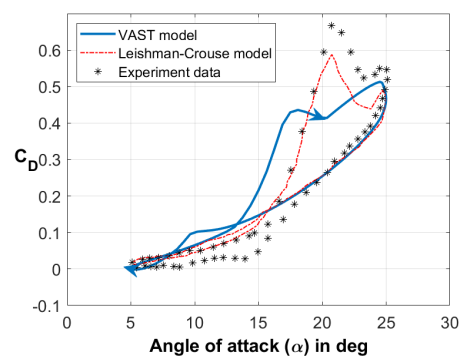
(d) Drag coefficient

Figure 4.5: Deep dynamic stall $\alpha = 15° + 10° \sin \omega t$; $k = 0.1$ and $M = 0.3$

Airfoil section	=	NACA 0012
Blade chord c	=	0.0767 m
Amplitude	=	0.174532925 rad
Amplitude offset	=	0.261799388 rad
Period	=	0.023623545 sec/cycle
Number of cycles	=	25 revolutions
Mach number	=	0.3
Reduced frequency (k)	=	0.1

Table 4.4: Deep dynamic stall configuration

to the experimental data when the critical conditions for the leading edge occur. The difference can be attributed to the vortex travel time adopted in the VAST. The rate at which vortex convection occurs is considered half of the free stream velocity in the VAST (Ref. [LB86]). Leishman and Crouse did not mention any specific value they considered in the model.

Figure 4.5b shows the pitching moment coefficient plot. The VAST model captures the qualitative trend during moment break but it lacks in capturing the values of experimental data and the Leishman-Crouse model. The difference in values of VAST model and experimental data mainly occurs after moment break and before down-stroke of the airfoil and this can be improved by re-evaluating the model for wake effects on pitching airfoil.

Figure 4.5d shows the drag coefficient plot. The VAST model captures the trend of the experimental and Leishman-Crouse data, but it does not realize full drag coefficient during the moment break. The second peak in experimental and Leishman-Crouse model is result of secondary vortex which requires a additional state to implement and it is not Incorporated in VAST model due to computational time.

Mach Number, M	0.30	0.40	0.50	0.60	0.70	0.75	0.80
$C_{L\alpha}$	0.108	0.113	0.117	0.127	0.154	0.175	0.216
α_1	15.25	12.5	10.5	8.5	5.6	3.5	0.7
$\Delta\alpha_1$	2.1	2.0	1.45	1.0	0.8	0.2	0.1
S_1	3.0	3.25	3.5	4.0	4.5	3.5	0.70
S_2	2.3	1.6	1.2	0.7	0.5	0.8	0.18
K_0	0.0025	0.006	0.02	0.038	0.030	0.001	-0.01
K_1	-0.135	-0.135	-0.125	-0.12	-0.09	-0.13	0.02
K_2	0.04	0.05	0.04	0.04	0.15	-0.02	-0.01
C_{D0}	0.0085	0.008	0.0077	0.0078	0.0078	0.0079	0.0114
D_f	8.0	7.75	6.2	6.0	5.9	5.5	4.0
C_{N1}	1.45	1.2	1.05	0.92	0.68	0.5	0.18
T_p	1.7	1.8	2.0	2.5	3.0	3.3	4.3
T_f	3.0	2.5	2.2	2.0	2.0	2.0	2.0
T_v	6.0	6.0	6.0	6.0	6.0	6.0	4.0
T_{vl}	7.0	9.0	9.0	9.0	9.0	9.0	9.0

Table 4.5: Airfoil coefficients used for unsteady aerodynamic modelling (Ref. [LB86]).

5 Conclusion and Outlook

Rotor aeroelasticity and performance analyses require versatile and relatively simple methods for evaluating the unsteady aerodynamics behavior of the blade sections. Therefore, the presented work developed a module to find the aerodynamic performance of a 2D airfoil section under non-linear and dynamic stall flow conditions. The output of this model is utilized by the VAST tool for rotor air loads analysis.

the VAST model is developed based on the state-space formulation given by Leishman and Crouse for the indicial method model presented by Leishman and Beddoes. In addition to the 12 states given by Leishman-Crouse in Ref. [Lei89], the VAST model utilizes two extra states. One state account for the non-dimensional vortex time travel constant over the airfoil chord, and the second one is to check for the change in the direction of the airfoil. Overall, the VAST model utilizes 14 states for the formulation used in the present work.

The attached flow model with indicial response function for the circulatory and non-circulatory components is implemented. Non-linear effects produced due to the Trailing Edge Separation (TES) are accounted by Kirchoff flow modification. A generalized stall boundary denoted the onset of the Leading Edge Separation (LES) or Shock-induced separation.

The VAST model is validated for stall onset and moderate and deep dynamic stall flow conditions, covering major dynamic stall ranges. The normal force coefficient show a qualitative trend almost similar to the experimental data and the Leishman-Crouse model for all the three test cases during the entire range of AoA. But it fails to realizes the full normal force coefficient during the stall break. The pitching moment coefficient shows a qualitative trend with experimental data and the Leishman-Crouse model. It captures the moment break at stall but lacks in capturing the qualitative magnitude of C_M.

Most of the differences between the model and the test data are apparent during the reattachment phase. However, in this regime, because of disturbances in the flow field, early and localized leading-edge reattachment takes place from cycle to cycle, and it is challenging to capture them.

Pitching moment formulation and implementation can be improved further by the implementation of modified separation point f_m for the reattachment of flow as suggested by Lieshman and Beddoes [LB86].

References

[Wag24]   H. Wagner. "Über die Entstehung des dynamischen Auftriebes von Tragflügeln". In: *VDI-Verl.(Berlin)* (1924).

[Küs36]   H.G. Küssner. "Zusammenfassender Bericht über den instationären Auftrieb von Flügeln". In: *Luftfahrtforschung* 13.12 (1936), pp. 410–424.

[KS38]   T.H. von Karman and W.R. Sears. "Airfoil theory for non-uniform motion". In: *Journal of the Aeronautical Sciences* 5.10 (1938), pp. 379–390.

[Jon40]   R.T. Jones. "The unsteady lift of a wing of finite aspect ratio". In: *NASA Washington DC* (1940).

[Sea41]   W.R. Sears. "On the reaction of an elastic wing to vertical gusts". In: *Journal of the Aeronautical Sciences* 8.2 (1941), pp. 64–67.

[The49]   T. Theodorsen. "General Theory Of Aerodynamic Instability And The Mechanism Of Flutter". In: *Classical Aerodynamic Theory* 1050 (1949), p. 291.

[Maz51]   B. Mazelsky. "Numerical determination of indicial lift of a two-dimensional sinking airfoil at subsonic Mach numbers from oscillatory lift coefficients with calculations for Mach number 0.7". In: *NASA Washington DC* (1951).

[Lom+52]   H. Lomax et al. "Two-and three-dimensional unsteady lift problems in high-speed flight". In: *NASA Washington DC* (1952).

[MD52]   B. Mazelsky and J.A. Drischler. "Numerical determination of indicial lift and moment functions for a two-dimensional sinking and pitching airfoil at Mach numbers 0.5 and 0.6". In: *NASA Washington DC* (1952).

[EM59]   W.T. Evans and K.W. Mort. "Analysis of computed flow parameters for a set of sudden stalls in low-speed two-dimensional flow". In: *NASA Washington DC* 85 (1959).

[SNS74]   R.M. Scruggs, J.F. Nash, and R.E. Singleton. "Analysis of dynamic stall using unsteady boundary-layer theory". In: *NASA Washington DC* (1974).

[Bed76]   T.S. Beddoes. "A synthesis of unsteady aerodynamic effects including stall hysteresis". In: *Vertica* 1.2 (1976), pp. 113–123.

[MCM76]   W.J. McCroskey, L.W. Carr, and K.W. McAlister. "Dynamic stall experiments on oscillating airfoils". In: *AIAA* 14.1 (1976), pp. 57–63.

[Bed78]   T.S. Beddoes. "Onset of leading edge separation effects under dynamic conditions and low Mach number". In: *American Heli-*

copter Society, Annual National Forum, 34 th, Washington DC (1978).

[Bed80]   T.S. Beddoes. "Unsteady flows associated with helicopter rotors". In: *AGARD Report* 679 (1980).

[Dow80]   E.H. Dowell. "A simple method for converting frequency domain aerodynamics to the time domain". In: *NASA Washington DC* (1980).

[TP80]   C.T. Tran and D. Petot. "Semi-empirical model for the dynamic stall of airfoils in view of the application to the calculation of responses of a helicopter blade in forward flight". In: *6th Eur Rotorcr Powered Lift Aircr Forum* (1980).

[Wil80]   M.H. Williams. "Unsteady thin airfoil theory for transonic flows with embedded shocks". In: *AIAA* 18.6 (1980), pp. 615–624.

[McC81]   W.J. McCroskey. "The phenomenon of dynamic stall". In: *NASA Washington DC* (1981).

[Bed82]   T.S. Beddoes. "Practical computation of unsteady lift". In: *8th Eur Rotorcr Powered Lift Aircr Forum* (1982).

[MP82]   W.J. McCroskey and S.L. Pucci. "Viscous-inviscid interaction on oscillating airfoils in subsonic flow". In: *AIAA* 20.2 (1982), pp. 167–174.

[McC+82]   W.J. McCroskey et al. "An Experimental Study of Dynamic Stall on Advanced Airfoil Sections. Volume 1. Summary of the Experiment." In: *NASA Washington DC* (1982).

[Bed83]   T.S. Beddoes. "Representation of airfoil behaviour". In: *Vertica* 7.2 (1983).

[Gan83]   S.T. Gangwani. "Synthesized airfoil data method for prediction of dynamic stall and unsteady airloads". In: *NASA Washington DC* (1983).

[Wil84]   P.G. Wilby. "An experimental investigation of the influence of a range of aerofoil design features on dynamic stall onset". In: *10th European rotorcraft forum* (1984).

[ZTF84]   R.E. Ziemer, W.H. Tranter, and D.R. Fannin. "Signals and systems: continous and discrete". In: *Prentice-Hall International Inc.* (1984).

[LB86]   J.G. Leishman and T.S. Beddoes. "A generalised model for airfoil unsteady aerodynamic behaviour and dynamic stall using the indicial method". In: *42nd Annual forum of the American Helicopter Society* 34 (1986), pp. 3–17.

[VF86]   C. Venkatesan and P.P. Friedmann. "New approach to finite-state modeling of unsteady aerodynamics". In: *AIAA* 24.12 (1986), pp. 1889–1897.

[Lei88]   J.G. Leishman. "Validation of approximate indicial aerodynamic functions for two-dimensional subsonic flow". In: *Journal of Aircraft* 25.10 (1988), pp. 914–922.

[Lei89]   J.G. Leishman. "State-space model for unsteady airfoil behavior and dynamic stall". In: *30th Structures, structural dynamics and materials conference* (1989), p. 1319.

[LC89]   J.G. Leishman and Jr.G. Crouse. "A state-space model of unsteady aerodynamics in a compressible flow for flutter analyses". In: *27th Aerospace Sciences Meeting* (1989), p. 22.

[Lei00]   J.G. Leishman. *Principles of helicopter aerodynamics*. Cambridge University Press, 2000, pp. 390–390.

[Woo11]   L.C. Woods. *The theory of subsonic plane flow*. Cambridge University Press, 2011.

[MR12]   K. Mulleners and M. Raffel. "The onset of dynamic stall revisited". In: *Experiments in fluids* 52.3 (2012), pp. 779–793.

[BAH13]   R.L. Bisplinghoff, H. Ashley, and R.L. Halfman. *Aeroelasticity*. Courier Corporation, 2013.

[Min18]   Maximilian Mindt. "Merging an Analytical Aerodynamic Model for Helicopter Applications with a State-Space Formulation for Unsteady Airfoil Behavior". In: *DLRK* (2018).

[Mir19]   K. Mirnal. *Theoretical and Experimental Aerodynamics*. Springer Nature Singapore Pte Ltd, 2019, pp. 127–143.

[Hof+20]   Johannes Hofmann et al. "VAST-Versatile Aeromechanics Simulation Platform For Helicopters". In: *DLRK* (2020).